

**ADSORPTION-PHOTOCATALYSIS OF MALACHITE GREEN USING
TITANIUM DIOXIDE AND EMPTY FRUIT BUNCH DERIVED-
ACTIVATED CARBON**

TEH WEN SHUN

**A project report submitted in partial fulfilment of the
requirements for the award of Bachelor of Engineering
(Hons.) Chemical Engineering**

**Lee Kong Chian Faculty of Engineering and Science
Universiti Tunku Abdul Rahman**

September 2017

DECLARATION

I hereby declare that this project report is based on my original work except for citations and quotations which have been duly acknowledged. I also declare that it has not been previously and concurrently submitted for any other degree or award at UTAR or other institutions.

Signature : _____

Name : _____

ID No. : _____

Date : _____

APPROVAL FOR SUBMISSION

I certify that this project report entitled “**ADSORPTION-PHOTOCATALYSIS OF MALACHITE GREEN USING TITANIUM DIOXIDE AND EMPTY FRUIT BUNCH-DERIVED ACTIVATED CARBON**” was prepared by **TEH WEN SHUN** has met the required standard for submission in partial fulfilment of the requirements for the award of Bachelor of Engineering (Hons.) Chemical Engineering at Universiti Tunku Abdul Rahman.

Approved by,

Signature : _____

Supervisor : _____

Date : _____

Signature : _____

Co-Supervisor : _____

Date : _____

The copyright of this report belongs to the author under the terms of the copyright Act 1987 as qualified by Intellectual Property Policy of Universiti Tunku Abdul Rahman. Due acknowledgement shall always be made of the use of any material contained in, or derived from, this report.

© 2017, Teh Wen Shun. All right reserved.

ACKNOWLEDGEMENTS

I would like to thank everyone who had contributed to the successful completion of this project. I would like to express my gratitude to my research supervisor, Dr. Pang Yean Ling for her invaluable advice, guidance and her enormous patience throughout the development of the research.

In addition, I would also like to express my gratitude to my loving parents, family and friends who had helped and given me encouragement and the necessary support to complete this project.

ABSTRACT

A novel AC/TiO₂ composite was synthesised using sol-gel method and were characterised using XRD, SEM-EDX, FT-IR, TGA and BET analysis. Anatase and rutile phase TiO₂ particles were successfully embedded on the AC surface in the composite and was mainly composed of Ti, O and C atoms. The AC/TiO₂ composite was made up of spherical TiO₂ particles agglomerated on the smooth tubular and porous structure of AC. The AC/TiO₂ composite had displayed significantly better performance in the photocatalytic degradation of Malachite Green as compared to pure AC and TiO₂. A few parameter studies such as various types of organic dyes, weight ratio of AC:TiO₂, catalyst loading, initial dye concentration and solution temperature were investigated to identify the optimum conditions for photocatalytic degradation. The photocatalytic efficiency was influenced by the weight proportion of AC:TiO₂ and the degradation process was attributed to the adsorption and photocatalysis processes. Using 2.5 g/L AC/TiO₂ at weight ratio 3:1 on an initial dye concentration of 10 mg/L at 50 °C, a degradation efficiency of 96.3 % was obtained in 7.5 minutes. Almost total removal of COD (96.7 %) was recorded. Reusability of AC/TiO₂ composite and kinetic study of the photodegradation of dye were also investigated. The recycled composite maintained high catalytic performance after one catalytic cycle. The degradation kinetics of Malachite Green at various solution temperatures were fitted to the pseudo first-order reactions and satisfactory results were obtained. The activation energy for the degradation of Malachite Green was 21.48 kJ/mol.

TABLE OF CONTENTS

DECLARATION	ii
APPROVAL FOR SUBMISSION	iii
ACKNOWLEDGEMENTS	v
ABSTRACT	vi
TABLE OF CONTENTS	vii
LIST OF TABLES	x
LIST OF FIGURES	xi
LIST OF SYMBOLS / ABBREVIATIONS	xiii
LIST OF APPENDICES	xvi

CHAPTER

1	INTRODUCTION	1
	1.1 Water Pollution in Malaysia	1
	1.2 Dye Production and Textile Industry	2
	1.3 Classifications of Dyes	2
	1.4 Environmental and Health Impacts	4
	1.5 Problem Statement	6
	1.6 Research Objectives	7
	1.7 Scope of Study	7
	1.8 Organisation of Thesis	8
2	LITERATURE REVIEW	9
	2.1 Colour Removal Technologies	9
	2.2 Heterogeneous Photocatalysis	13
	2.3 Semiconductor Photocatalysts	15
	2.4 Synthesis Method of AC/TiO ₂ Photocatalyst	19
	2.5 Characterisation Study	21

2.6	Kinetics of Photocatalytic Degradation	23
2.7	Parameters Influencing the Photocatalytic Degradation	24
2.7.1	Effect of Various Types of Organic Dyes	24
2.7.2	Effect of AC/TiO ₂ Composite at Different Weight Ratio	25
2.7.3	Effect of Catalyst Loading	25
2.7.4	Effect of Solution pH	26
2.7.5	Effect of Initial Dye Concentration	26
2.7.6	Effect of Solution Temperature	27
3	METHODOLOGY AND WORK PLAN	29
3.1	Materials and Chemicals	29
3.2	Equipment	32
3.3	Overall Flowchart of Research	32
3.4	Experimental Setup	32
3.5	Preparation of Catalyst	35
3.5.1	Preparation of Activated Carbon	35
3.5.2	Preparation of AC/TiO ₂ Composite	36
3.6	Characterisation of Photocatalysts	36
3.6.1	XRD	36
3.6.2	SEM-EDX	37
3.6.3	FT-IR Spectroscopy	37
3.6.4	TGA	37
3.6.5	BET Analysis	37
3.7	Parameter Studies	38
3.7.1	Effect of Various Types of Organic Dyes	38
3.7.2	Effect of AC/TiO ₂ Composite at Different Weight Ratio	38
3.7.3	Effect of Catalyst Loading	39
3.7.4	Effect of Initial Dye Concentration	39
3.7.5	Effect of Solution Temperature	39
3.8	Reusability Study	40
3.9	Kinetic Study	40

3.10	Liquid Sample Analysis	41
4	RESULTS AND DISCUSSIONS	43
4.1	Characterisation of Photocatalysts	43
4.1.1	XRD	43
4.1.2	SEM-EDX	45
4.1.3	FT-IR Spectroscopy	47
4.1.4	TGA	48
4.1.5	BET Analysis	50
4.2	Parameter Studies	50
4.2.1	Effect of Various Types of Organic Dyes	50
4.2.2	Adsorption and Photocatalytic Performance of AC/TiO ₂ Composites	52
4.2.3	Effect of Catalyst Loading	54
4.2.4	Effect of Initial Dye Concentration	55
4.2.5	Effect of Solution Temperature	56
4.3	Reusability Study	57
4.4	Kinetic Study	58
4.5	Liquid Sample Analysis	61
4.5.1	COD Results	61
5	CONCLUSIONS AND RECOMMENDATIONS	63
5.1	Conclusions	63
5.2	Recommendations for future work	64
	REFERENCES	65
	APPENDICES	76

LIST OF TABLES

Table 1.1:	Typical Textile Effluent Characteristics and Standards for Effluent Discharge (Department of Environment Malaysia, 2010)	3
Table 1.2:	Degree of Fixation for Different Dye-Fibre Combinations (Choudhury, 2006)	4
Table 1.3:	Properties, Principal Chemical Classes and Applications for Various Types of Dyes (Clark, 2011; Hunger, 2003)	5
Table 2.1:	Benefits and Drawbacks of Physical and Chemical Methods of Dye Removal (Ramachandran, et al., 2013)	10
Table 3.1:	List of Chemical Used and its Specifications	29
Table 3.2:	The Chemical Properties of Model Pollutant Used in Research (Kamalakkannan, et al., 2015)	30
Table 3.3:	List of Equipment Used and its Respective Function	33
Table 4.1:	Average Crystallite Sizes for Pure TiO ₂ , AC and AC/TiO ₂ at Various Weight Ratio	44
Table 4.2:	Distribution of Elements in Various Samples	47
Table 4.3:	Reaction Rate Constants for Photocatalytic Degradation of Malachite Green by AC/TiO ₂ Composite at Weight Ratio 3:1 under Different Solution Temperatures	60

LIST OF FIGURES

Figure 1.1:	Trend of River Quality in Malaysia from 2011-2015 (Department of Environment Malaysia, 2015)	1
Figure 2.1:	General Mechanism of Photocatalysis (Ahmed, et al., 2010)	14
Figure 2.2:	Band Gap Energies of Semiconductors on a Potential Scale (V) against the Normal Hydrogen Electrode (NHE) (Mano, et al., 2015)	16
Figure 2.3:	Structures of TiO ₂ , (a) Anatase, (b) Brookite, (c) Rutile (Liu, et al., 2013)	16
Figure 3.1:	Flowchart of Overall Research Activities	34
Figure 3.2:	Schematic Diagram of the Experimental Setup (1) Power Socket Adaptor, (2) Fluorescent Bulb, (3) Retort Stand with Clamp, (4) Aluminium Foil, (5) Beaker, (6) Hot Plate Magnetic Stirrer, (7) Magnetic Stir Bar	35
Figure 4.1:	XRD Patterns for (a) Pure TiO ₂ , AC/TiO ₂ Composite at Weight Ratio (b) 1:3, (c) 1:1, (d) 3:1 and (e) Pure AC	43
Figure 4.2:	SEM Images of (a) Pure TiO ₂ , AC/TiO ₂ Composite at Weight Ratio (b) 1:3, (c) 1:1, (d) 3:1 and (e) Pure AC	46
Figure 4.3:	FT-IR Spectra for (a) Pure AC, AC/TiO ₂ Composite at Weight Ratio (b) 1:3, (c) 1:1, (d) 3:1 and (e) Pure AC	48
Figure 4.4:	TGA Curves for (a) Pure TiO ₂ , (b) AC/TiO ₂ Composite at Weight Ratio 1:3 and (c) Pure AC	49
Figure 4.5:	Photocatalytic Degradation of Various Organic Dyes by AC/TiO ₂ Composite at Weight Ratio 3:1 (Catalyst Loading = 2.5 g/L, Initial Dye Concentration = 10 mg/L, Solution Temperature = 50 °C, Reaction Time = 7.5 minutes)	51
Figure 4.6:	Adsorption Capacity of Malachite Green by Pure AC, TiO ₂ and AC/TiO ₂ Composite at Various Weight Ratio (Catalyst Loading = 2.5 g/L, Initial	

	Dye Concentration = 10 mg/L, Solution Temperature = 30 °C, Reaction Time = 30 minutes)	52
Figure 4.7:	Photocatalytic Degradation of Malachite Green by Pure AC, TiO ₂ and AC TiO ₂ Composite at Various Weight Ratio (Catalyst Loading = 2.5 g/L, Initial Dye Concentration = 10 mg/L, Solution Temperature = 30 °C, Reaction Time = 30 minutes)	53
Figure 4.8:	Effect of Catalyst Loading on the Photocatalytic Degradation of Malachite Green in the Presence of AC/TiO ₂ Catalyst at Weight Ratio 3:1 (Initial Dye Concentration = 10 mg/L, Solution Temperature = 30 °C, Reaction Time = 30 minutes)	55
Figure 4.9:	Effect of Initial Dye Concentration on the Photocatalytic Degradation of Malachite Green in the Presence of AC/TiO ₂ Catalyst at Weight Ratio 3:1 (Catalyst Loading = 2.5 g/L, Solution Temperature = 30 °C, Reaction Time = 30 minutes)	56
Figure 4.10:	Effect of Solution Temperature on the Photocatalytic Degradation of Malachite in the Presence of AC/TiO ₂ Catalyst at Weight Ratio 3:1 (Catalyst Loading = 2.5 g/L, Initial Dye Concentration = 10 mg/L, Reaction Time = 7.5 minutes)	57
Figure 4.11:	Photocatalytic Degradation of Malachite Green by Fresh and Reused AC/TiO ₂ Catalyst at Weight Ratio 3:1 (Catalyst Loading = 2.5 g/L, Initial Dye Concentration = 10 mg/L, Solution Temperature = 50 °C, Reaction Time = 30 minutes)	58
Figure 4.12:	Pseudo First-Order Reaction Kinetics Plot for Photocatalytic Degradation of Malachite Green	59
Figure 4.13:	Arrhenius Plot of ln k _{app} against 1/T	61

LIST OF SYMBOLS / ABBREVIATIONS

A	pre-exponential constant, min^{-1}
C	concentration of the dye at any time, $\frac{\text{mg}}{\text{L}}$
C_0	initial dye concentration, $\frac{\text{mg}}{\text{L}}$
C_t	dye concentration at time t , $\frac{\text{mg}}{\text{L}}$
D	average crystalline size
E_a	activation energy, J/mol
K	adsorption coefficient of the dye, $\frac{\text{mg}}{\text{L}}$
K	Scherrer constant
k_0	apparent pseudo zero-order rate constant, $\frac{\text{mg}}{\text{L}\cdot\text{min}}$
k_1	apparent pseudo first-order rate constant, min^{-1}
k_2	apparent pseudo second-order rate constant, $\frac{\text{L}}{\text{mg}\cdot\text{min}}$
k_{app}	reaction rate constant
R	gas constant, 8.314 J/mol·K
r	oxidation rate of the dye, $\frac{\text{mg}}{\text{L}\cdot\text{min}}$
t	illumination time, min
T	temperature, K
β	the peak width of half maximum
θ	Bragg diffraction angle
λ	X-ray wavelength
AATC	American Association of Textile Chemistry and Colourists
AC	activated carbon
Ag	silver
AOP	advanced oxidation process
ATR	attenuated total reflectance
Au	gold
BET	Brunauer-Emmett-Teller
BOD	biological oxygen demand
C	carbon atom
C. I.	colour index
CB	conduction band

Cl	chlorine atom
Co	cobalt atom
CO ₂	carbon dioxide
COD	chemical oxygen demand
CuO	copper oxide
e ⁻	electron
EFB	empty fruit bunch
Fe	iron
FT-IR	Fourier transformed infrared
H	hydrogen atom
h ⁺	hole
H ₂ O	water molecule
H ₂ O ₂	hydrogen peroxide
HO ₂ [·]	superoxide radical anion
<i>hν</i>	photon
K	potassium atom
KOH	potassium hydroxide
MgO	magnesium oxide
MOCVD	metal organic chemical vapour deposition
N	nitrogen atom
NHE	normal hydrogen electrode
Ni	nickel atom
O	oxygen atom
O ₂	oxygen molecule
OH [·]	hydroxyl radical
Pd	palladium
Pt	platinum
SEM-EDX	scanning electron microscopy- energy dispersive x-ray
Si	silicon
SnO ₂	tin dioxide
TDS	total dissolved solids, $\frac{\text{mg}}{\text{L}}$
TGA	thermogravimetric analysis
TiO ₂	titanium dioxide

TSS	total suspended solids, $\frac{\text{mg}}{\text{L}}$
TTIP	titanium (IV) isopropoxide
UV	ultraviolet
UV-Vis	ultraviolet/ visible
VB	valence band
WO ₃	tungsten trioxide
XRD	x-ray diffraction
Zn	zinc
ZnO	zinc oxide

LIST OF APPENDICES

APPENDIX A: EDX Analysis	76
APPENDIX B: Preparation of Various Concentrations of Organic Dyes	77
APPENDIX C: Calibration Curve of Malachite Green	79
APPENDIX D: Calculation of Average Crystallite Sizes	80
APPENDIX E: Reaction Kinetics Plot	81
APPENDIX F: Material Safety Data Sheet (MSDS)	83

CHAPTER 1

INTRODUCTION

1.1 Water Pollution in Malaysia

Water pollution is becoming a major worldwide problem especially with the rapid development that is ongoing today. According to Figure 1.1, the number of slightly polluted and polluted rivers in Malaysia has been increasing. Although there were improvements in 2015, the figures for dirty river remained high. The main source of these high figures was deemed to be insufficient sewage treatment or effluent from agro-based and manufacturing industries (Department of Environment Malaysia, 2015).

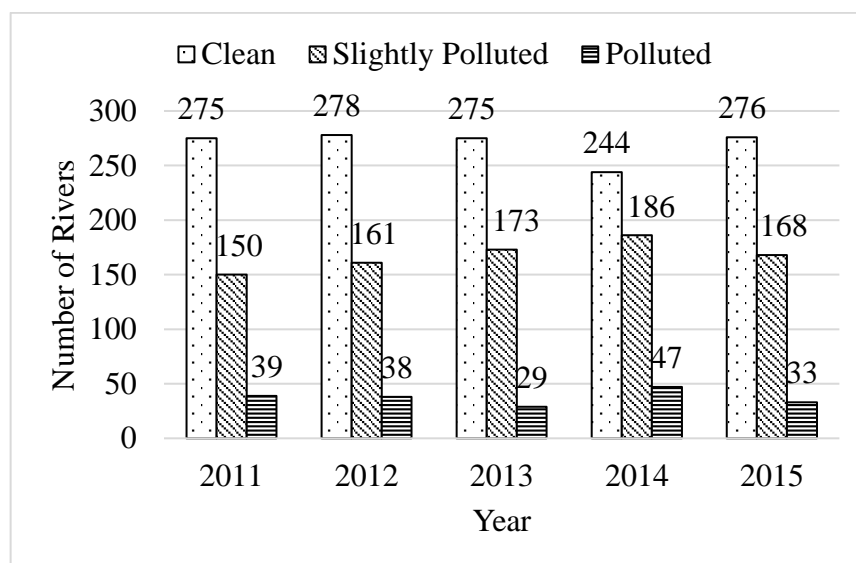


Figure 1.1: Trend of River Quality in Malaysia from 2011-2015 (Department of Environment Malaysia, 2015)

Out of the total volume of industrial wastewater produced in Malaysia, 22 % of it came from textile finishing (Yeoh, et al., 1993). In addition, water consumption level can reach as high as 500 litres per kilogram of textile produced in the textile industry (Kalliala and Talvenmaa, 2000). This large volume of water used can contribute to serious environmental problems if it is not treated properly.

1.2 Dye Production and Textile Industry

Dye is a natural or synthetic substance used to give colour and change the appearance of a substrate. Dyes are utilised in many industries such as textile, plastic, paper and so forth. It is estimated that over 10 000 different dyes and pigments utilised industrially and over 700 000 tonnes of synthetic dyes are manufactured each year globally (Gürses, et al., 2016). According to IBP (2016), the textile industry consumes almost 70 % of the total production. It is estimated that up to 200 000 tonnes of dyes are lost to textile industry effluents each year because of the non-optimal dyeing procedure (Günay, 2013).

Table 1.1 depicts the typical characteristics of textile effluent and the regulations of discharge industrial effluent in Malaysia. Industrial effluents are required to conform to Standard A or B under environmental regulations depending on the point of discharge (Department of Environment Malaysia, 2010). It can be observed that the quality obtained from textile effluent is far off than the acceptable values as stipulated by Standard A or B. This suggests that proper treatment methods need to be employed before discharging so that it will not severely impact the environment.

1.3 Classifications of Dyes

Dye molecules have two key components: chromophores and auxochromes. Each component has a different function. Chromophores give colour to the dye, while auxochromes help to enhance the chromophores. This enable the molecules to be soluble in water and increase the affinity of dye towards fibres (Gupta and Suhas, 2009).

In general, there are two ways to classify dyes; based on their molecular structure and their application to the fibre type (Hunger, 2003). Dyes have different classes such as direct, vat, sulphur, azo, reactive, acid, disperse and basic dyes (Clark, 2011). Hunger (2003) claimed that classifying dyes based on application was easier than based on chemical structures because of the complex nomenclatures used in the former system. Besides, classification by application is the main system used in the Colour Index (C.I.). The C.I. is a popular classification system devised by the Society of Dyers and Colourists in collaboration with the American Association of Textile Chemists and Colourists (AATC). It has an extensive glossary of dyes and pigments together with their respective structures and applications (Clark, 2011).

Table 1.1: Typical Textile Effluent Characteristics and Standards for Effluent Discharge (Department of Environment Malaysia, 2010)

Parameter	Unit	Typical range ^a	Standard	Standard
			A ^b	B ^b
Biological oxygen demand (BOD ₅ at 20 °C)	mg/L	200-300	20	40
Chemical oxygen demand (COD)	mg/L	50-5000	80	250
Colour	ADMI ^c	NA	100	200
Organic nitrogen	mg/L	18-39	NA	NA
pH	NA	2-10	6-9	5.5-9
Temperature	°C	30-80	40	40
Total chromium	mg/L	0.2-0.5	0.05	0.05
Total dissolved solids (TDS)	mg/L	1500-2200	NA	NA
Total phosphorus	mg/L	0.3-15	NA	NA
Total suspended solids (TSS)	mg/L	50-500	50	100

NA not available

^a Data obtained from Marcucci, et al. (2003)

^b Extracted from Environmental Quality (Industrial Effluents) Regulations 2009 (PU (A) 434). Standard A is referred to the effluent discharged to the upstream of surface or above subsurface water supply intakes. Standard B is referred to any other inland water.

^c Stands for American Dye Manufacturers Institute.

Generally, the amount of dye in the effluent is closely linked to the fixation rates of the various dyes and fibres (Choudhury, 2006). The degree of fixation with respect to different dyes can be seen in Table 1.2. It can be inferred that basic dyes have the highest fixation rate while reactive dyes have the lowest fixation rate. The loss of reactive dyes happens because they are not completely used up during the dyeing process and some are hydrolysed in the alkaline dye bath. Dye hydrolyses when it reacts with water instead of reacting with the functional group of textile fabrics (Lau and Ismail, 2009). In addition, both reactive dyes and their hydrolysed form are not biodegradable and hence can cause water contamination easily (Gupta and Suhas, 2009).

Table 1.2: Degree of Fixation for Different Dye-Fibre Combinations (Choudhury, 2006)

Dye application class	Fibre	Degree of fixation (%)	Lost to effluent (%)
Acid	Polyamide	80-95	5-20
Basic	Acrylic	95-100	0-5
Direct	Cellulose	70-95	5-30
Disperse	Polyester	90-100	0-10
Metal-complex	Wool	90-98	2-10
Reactive	Cellulose	50-90	10-50
Sulphur	Cellulose	60-90	10-40
Vat	Cellulose	80-95	5-20

Table 1.3 lists out the properties, principal chemical classes and applications for a few types of dyes. Among all the principle classes in Table 1.3, the most commonly used are azo dyes. In fact, they account for 60-70 % of the total dyes produced (Gupta and Suhas, 2009). According to Roessler and Jin (2003), reactive dyes (50 %) are used for most of the colouration of cellulosic fibres, followed by vat dyes (17 %), indigo dyes (7 %), sulphur dyes (7 %), and finally naphthole dyes (3 %).

1.4 Environmental and Health Impacts

In general, there are two types of textile mills: dry processing mills and wet processing mills. Wastes generated in dry processing mills are usually in solid form while all sorts of wastewater are generated in the wet processing mills through processes like desizing, scouring, bleaching, mercerising, dyeing, printing, and finishing (Verma, et al., 2012).

Textile wastewater from various stages of processing composed of many pollutants and can disturb the ecological environment if not treated properly. The obvious problem is that these wastes change the colour of the water bodies and can be an eyesore to the public (Verma, et al., 2012). Besides, it also prevents sunlight from reaching the bottom of the river and hence disturbs the ecosystem (Georgiou, et al., 2002). Not only that, groundwater systems are also impacted due to the leaching from soil (Namasivayam and Sumithra, 2005).

Table 1.3: Properties, Principal Chemical Classes and Applications for Various Types of Dyes (Clark, 2011; Hunger, 2003)

Type of dye	Properties	Principle chemical classes	Main applications
Acid	Water-soluble	Azo (including premetallized), anthraquinone, azine, nitro, xanthene, triphenylmethane and nitroso	Wool, paper, nylon, silk, inks and leather
Azo	Water-insoluble	Azo	Cotton, rayon, polyester and cellulose acetate
Basic	Water-soluble	Diazahemicyanine, triarylmethane, cyanine, hemicyanine, thiazine, oxazine, diphenylmethane, azo, azine, xanthene and acridine	Paper, polyacrylonitrile, modified polyester, nylon and inks
Direct	Water-soluble	Phthalocyanine, azo, stilbene and oxazine	Dyeing of cotton, paper, nylon and leather
Disperse	Water-insoluble	Azo, anthraquinone, nitro, styryl and benzodifuranone	Polyester, acetate, plastics, acrylic and polyamide
Reactive	Form covalent bond with fibre	Phthalocyanine, oxazine, anthraquinone, azo, formazan and basic	Cotton, silk, nylon and wool
Sulphur	Produced from aromatic intermediates	Azo, anthraquinone, phthalocyanine and triarylmethane	Plastics, gasoline, lubricants, oils and waxes
Vat	Water-insoluble	Anthraquinone (including polycyclic quinones) and indigoids	Cotton, wool and rayon

Many of the dyes were found to be toxic to aquatic life and harmful to human because it could cause mutations and carcinogenic characteristics (Ma, et al., 2017). Studies had shown that sporadic and excessive exposure to textile wastewater can cause many health complications such as leukaemia, multiple myeloma, profuse diarrhoea and tissue necrosis (Foo and Hameed, 2010).

1.5 Problem Statement

Water pollution caused by the textile industry is mainly because of the loss of dye effluents into the water bodies as a result of low degree of fixation. These wastewater effluents are not only an eyesore but can also cause harmful effects to the environment and human being as well. Currently, many treatment plants in Malaysia employ treatment methods such as biological method alone or physical methods coupled with a biological method to treat the textile effluents (Pang and Abdullah, 2013). However, such techniques are only effective up to a certain point and have their own disadvantages. For example, biological treatments had been proven to have little effect on dye removal.

Based on a review by Gupta and Suhas (2009), promising results can be obtained from dye removal methods such as adsorption or a mixture of processes involving adsorption. Despite their effectiveness, adsorbents such as activated carbons (ACs) are not exactly cheap. Not only that, the regeneration is costly and involve the loss of adsorbent. In light of that, many researchers have tried to find alternative inexpensive adsorbents. Currently, biomass and other waste materials having little or no economic value can actually be converted to AC that serves as an alternative to commercial ACs (Rafatullah, et al., 2010). Despite that, some researchers found that adsorption was only able to transfer the pollutants from one phase to another rather than totally eliminating them (Asiltürk and Sener, 2012). Hence, this is not a complete solution.

Other alternatives to treat recalcitrant and non-biodegradable compounds in water are advanced oxidation processes (AOPs) such as photocatalytic oxidation. Specifically, heterogeneous photocatalysis using Titanium Dioxide (TiO_2) suspension has better prospects among AOPs in eliminating low concentration contaminants with the assist of artificial or natural light (Palominos, et al., 2009). However, the use of powdered TiO_2 also has its disadvantages. It is difficult to be separated from the aqueous solution, susceptible to aggregation at high

concentrations and hard to be recycled (Asiltürk and Sener, 2012). One way to approach this problem is by immobilising TiO_2 on an inert and suitable supporting matrix (Asiltürk and Sener, 2012). Several support matrices have been investigated in the past but ACs might lead the rest as a better support because of their high surface area, robust and stable structure and composition (Leary and Westwood, 2011).

Therefore, this project proposes to address these issues by conducting a study on the photocatalytic degradation of synthetic dyes using AC/ TiO_2 composite and observing the degradation behaviour of the dye. The composite was prepared using TiO_2 synthesised by sol-gel method and AC obtained from empty fruit bunch fibres. The characteristic of the composite material was investigated and its photocatalytic properties were compared with AC and bare TiO_2 . On top of that, the operating parameters such as weight ratio of AC/ TiO_2 , catalyst loading, initial dye concentration, solution temperature and various types of organic dyes were varied to identify the impacts to the photocatalytic degradation rate. The reusability of the composite was also studied. Lastly, kinetics study was performed on the photocatalytic degradation process.

1.6 Research Objectives

The main goal of this research is to produce a novel AC/ TiO_2 composite for the purpose of photocatalytic degradation of Malachite Green. Specific objectives of this research include:

- i. To synthesise and characterise AC/ TiO_2 composite using sol-gel method.
- ii. To investigate the process behaviour of photocatalytic degradation under various operating parameters.
- iii. To investigate the reusability of the AC/ TiO_2 composite.
- iv. To study the reaction kinetic orders for photocatalytic degradation process.

1.7 Scope of Study

AC/ TiO_2 composite was synthesised using sol-gel method. Then, the composite material was characterised using X-ray Diffraction (XRD), scanning electron microscopy- energy dispersive X-ray analysis (SEM-EDX), Fourier transformed infrared (FT-IR) spectroscopy, thermogravimetric analysis (TGA) and Brunauer-Emmett-Teller (BET) analysis.

After that, a series of experiments were carried out using AC/TiO₂ composite in the photocatalytic degradation of Malachite Green. Various parameters were tested during experiments such as weight ratio of AC/TiO₂, catalyst loading, initial dye concentration, solution temperature and various types of organic dyes.

1.8 Organisation of Thesis

The thesis is divided into 5 chapters. Chapter 1 covers the situation of water pollution in Malaysia, the dye production and textile industry, classifications of dyes as well as the environmental and health impacts of untreated dye. The problem statement clearly highlights the need for this study. The objectives list out the problems that need to be studied and solved through this study. The scope of study describes the details of the objectives and research work done in this study.

Chapter 2 consists of literature reviews on the colour removal technologies and photocatalytic degradation, basic properties of TiO₂, ACs and possible mechanisms for photocatalytic degradation. The reported literature also points out the main factors influencing photocatalytic degradation.

Chapter 3 provides information about the research methodology. All information of the materials and chemical reagents utilised are listed. The details of the preparation of AC/TiO₂ composite are described in this chapter. The experimental setup and methods used in the characterisation of the catalysts are also described.

Chapter 4 deals with the results and discussion of the study. It consists of the characterisation of the catalysts, process study on factors influencing photocatalytic degradation, reaction kinetics of degradation and reusability study of the catalysts.

Chapter 5 gives the summary of the entire study. It presents the conclusions achieved in the study and recommendations for future work based on the obtained results and conclusions.

CHAPTER 2

LITERATURE REVIEW

2.1 Colour Removal Technologies

Over the past few years, there have been growing interests in the methods of decolourising textile effluents especially reactive azo dyes that constitute about 30 % of the entire dye market (Ramachandran, et al., 2013). This is partly because of the rising environmental concerns as well as the obligation of meeting the stringent international standards for discharging wastewater. These methods range from physical, chemical, biological processes and also more novel methods like AOPs. Nevertheless, all these methods possess their own sets of benefits and drawbacks. Hence, a combination of these methods is usually required to yield a satisfactory colour removal. Table 2.1 shows the benefits and drawbacks for some of the physical and chemical methods employed in treating coloured effluents.

There are many physical treatment methods proposed by various researchers. One of them is adsorption which is a colour elimination method that depends on the attraction of various dyes on adsorbents. The dye molecules will accumulate at the gas-solid or liquid-solid interfaces. Some of the factors that can affect the efficiency of the adsorption process are the surface area of the adsorbent, dye-adsorbent interactions, size of the adsorbent particle, temperature, pH, contact time and the ratio of adsorbent to dye (Yagub, et al., 2014). One of the most common and effective adsorbent used is AC. However, such method requires high maintenance costs, pre-treatment of wastewater to reduce the suspended solid content to acceptable range before entering the adsorption column, and a proper way to dispose the used adsorbents (Bazrafshan, et al., 2015).

Besides that, there are also filtration systems such as microfiltration, nanofiltration, ultrafiltration and reverse osmosis. Among these few methods, nanofiltration is most suitable to remove dyes from textile effluents because it performs well under relatively milder conditions (Mezohegyi, et al., 2012). In addition, membrane technology is also utilised in the removal of dyes from textile effluents. According to Verma, et al. (2012), these methods can filter and recycle pigment-rich wastewater, bleaching and mercerising wastewater. However, some limitations of these methods are regular membrane fouling, high expenses, the

Table 2.1: Benefits and Drawbacks of Physical and Chemical Methods of Dye Removal (Ramachandran, et al., 2013)

Physical/ Chemical Methods	Benefits	Drawbacks
Activated carbon	Good removal of many types of dyes	High cost
Advanced oxidation processes	Zero sludge production, minimal consumption of chemicals and efficient in treating recalcitrant dyes	Economically impractical
Chemical coagulation/ flocculation	Simple and economical	High quantity of sludge generation and not effective for soluble dyes
Electrochemical destruction	Breakdown compounds are harmless	High electricity expenses
Fenton's reagent	High effectiveness in decolourising both soluble and insoluble dyes	Sludge generation
Ion exchange	No adsorbent loss due to regeneration	Ineffective for all dyes
Irradiation	Effective oxidation at lab scale	Requires a lot of dissolved oxygen
Membrane filtration	Removes all types of dyes	Concentrated sludge production
Ozonation	No alteration of volume due to application in gaseous state	Short half-life (20 min)
Photochemical	No sludge generation	Formation of by-products

requirement of disposing the leftover concentrated dyebath properly and the need for different pre-treatment of influent wastewater. Moreover, the membrane's lifetime is usually short and thus requires proper pre-treatment units to treat the suspended

solids in wastewater to prolong the lifetime (Verma, et al., 2012). All these extra costs make filtration a less favourable choice to treat real wastewater.

Another physical method of treating wastewater is ion exchange. Here, exchange process occurred between the target ion that is transferred to a synthetic resin and a similarly charged presaturant ion that diffuses into the solution (Victor-Ortega, et al., 2017). This is not a popular method because it is only effective on basic, acid, direct and reactive dyes but not non-ionic dyes such as dispersive dyes (Pang and Abdullah, 2013). The benefits of this method are the ability to eliminate soluble dyes, recovery of used solvent and no loss of adsorbent on regeneration. However, this method is quite costly because of the high price of organic solvents (Robinson, et al., 2001).

On top of that, chemical coagulation or flocculation is also used to treat wastewater. Based on Verma, et al. (2012), it encompasses the use of chemicals to modify the physical state of suspended and dissolved solids with the objective of making it easy for removal by sedimentation. Some of the chemicals used include inorganic coagulants such as ferrous sulphate and aluminium sulphate (Mezohegyi, et al., 2012). This method is used as pre-treatment or main treatment of textile effluents containing dyes because it is relatively cheap. However, this method generates large quantity of sludge and is ineffective in treating soluble dyes (Verma, et al., 2012).

For the purpose of getting rid of dye from textile effluents, conventional physical and chemical techniques such as filtration, coagulation by chemical agents, adsorption on activated carbon, ion exchange on synthetic adsorbent resins and so forth are efficient up to a certain extent. For example, adsorption merely changes the phase of the pollutants from one to another without entirely eliminating it and hence producing secondary pollutants along the way (Asiltürk and Sener, 2012). This method generates a lot of sludge which needs to be removed and thus resulting in higher cost of wastewater treatment.

As for biological treatment, microorganisms are used to degrade organic dyes by using fixed or suspended growth systems through aerobic or anaerobic conditions. Aerobic implies the presence of oxygen while anaerobic implies its absence. Some example of microorganisms used in biological treatment are yeasts, algae and bacteria. These microscopic organisms can process the biodegradable organic into water, energy and carbon dioxide (CO₂) (Pang and Abdullah, 2013). According to

Tomei, et al. (2016), dyes especially reactive azo dyes are hard to be biodegraded because of the complex structure. Many bacteria need to be used to break down the strong nitrogen double bond. The products of the degradation are colourless aromatic amine by-products which are toxic (Tomei, et al., 2016). Based on Pang and Abdullah (2013), the acclimatisation time is usually very long due to the microorganism having a slow growth rate hence making this a slow process. On the flip side, this method creates methane gas which can be used for other purposes (Pang and Abdullah, 2013).

Besides that, the BOD₅/ COD ratio of textile wastewater is usually in the range of 0.06 and 0.35. For substances having a ratio smaller than 0.4, it is not easily biodegradable and hence biological treatments are not efficient for textile wastewater (Bilinska, et al., 2016). Moreover, biological treatment is not suitable for eliminating colours and dissolved ions from textile wastewater (Mokhtar, et al., 2016).

In addition, chemical oxidation process such as ozonation is appropriate for removing colours from textile effluents because it can break down organic matters resistant to biodegradation. Double bonds present in chromophore groups can be removed by ozone (Morali, et al., 2016). Ozonation addresses the limitations of the chemical and biological treatment methods because it results in satisfactory removal of dyes and decrease in chemical oxygen demand (COD) (Quan, et al., 2017). According to Robinson, et al. (2001), one major benefit of ozonation is that ozone can be applied in its gaseous state and will not increase the volume of sludge and wastewater. However, ozonation has a short half-life. This duration can get even shorter when there is the presence of organic pollutant and the stability of the process is influenced by the presence of pH, salts and temperature (Robinson, et al., 2001). Besides, acidic compounds which are difficult to be treated by ozonation can be produced if the pH of the liquid phase is too low and thus ozonation is usually coupled with other methods such as UV, H₂O₂ and TiO₂ to treat wastewater (Quan, et al., 2017).

Recently, there are also novel methods such as AOPs that produce extremely reactive species like hydroxyl radicals that are effective in degrading many types of organic pollutants rapidly and non-selectively (Dulov, et al., 2011). AOPs can degrade organic pollutants completely into harmless substances such as water, carbon dioxide and inorganic ions. Heterogeneous photocatalysis is one of the example for AOPs. Here, TiO₂ has the highest potential as a catalyst for wastewater

treatment because of its excellent properties such as high physicochemical stability, high reactivity, non-toxicity and relatively cheap price. However, there are a few limitations of TiO₂ such as the limited range of wavelengths for activation and high rate of electron-hole recombination (Nasirian, et al., 2017).

2.2 Heterogeneous Photocatalysis

Homogeneous catalysis are reactions that are catalysed by a catalyst that has the same phase as the reactants. On the other hand, heterogeneous catalysis involves reactants and catalyst of different phases. The latter is more desirable since it is easier to separate the catalyst from the solution after catalysis reaction. Heterogeneous catalysis covers five steps: (1) diffusion of reactant molecules from bulk solution to the surface, (2) adsorption of reactants onto the surface, (3) reaction on the surface, (4) desorption of products from the surface and (5) diffusion of products to the bulk solution (Unnikrishnan and Srinivas, 2016).

In general, photocatalysis encompasses the process of photosensitization where a chemical reaction happens because of the absorption of photonic energy by another chemical species referred to as photosensitizer, normally a semiconductor (Mills and Le Hunte, 1997). Semiconductors such as iron oxide, titanium dioxide, zinc sulphide and zinc oxide are suitable to act as photosensitizers because they have the special configuration of a filled valence band and an empty conduction band (Akpan and Hameed, 2009).

The general mechanism of a photocatalytic process using TiO₂ as catalyst is shown in Figure 2.1 (Ahmed, et al., 2010). Based on Ragupathy, et al. (2015) and Ahmed, et al. (2010), the incoming photons ($h\nu$) with energy equal or larger than the band gap value are absorbed by the photocatalyst particles. If the energy is lower than the band gap value, heat will usually be released. The photons will result in the promotion of an electron (e^-) to the conduction band (CB), leaving behind a positive hole (h^+) in the valence band (VB). The electron in the CB can either oxidize the dye directly or react with the adsorbed oxygen and water to form a superoxide radical anion. At the same time, the hole in the VB can either oxidize the dye directly or react with hydroxyl radical or water to form hydroxyl radical. The hydroxyl radical and other radicals are responsible for heterogeneous photocatalysis process. The entire process can be represented by reactions 2.1 to 2.8.

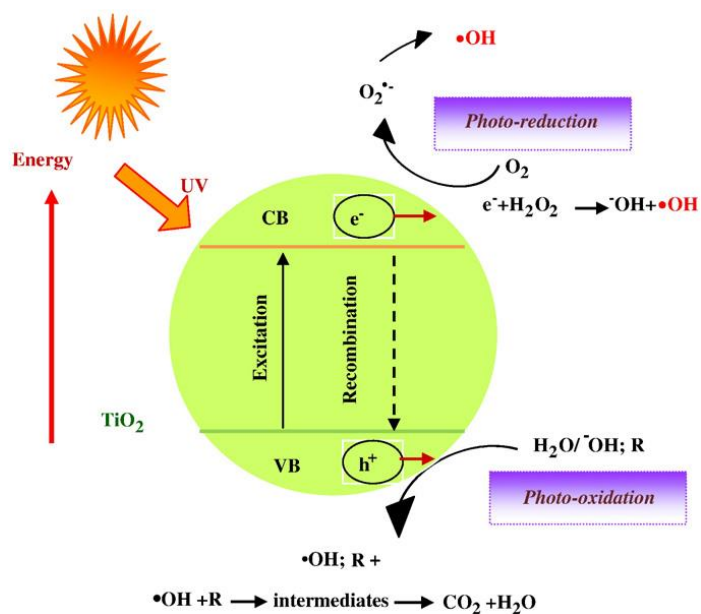
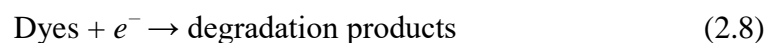
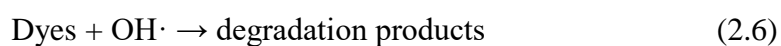
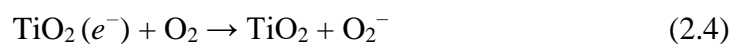
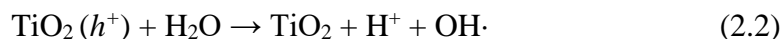
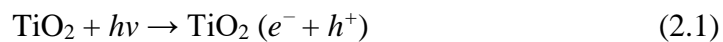


Figure 2.1: General Mechanism of Photocatalysis (Ahmed, et al., 2010)

It should be noted that if the reduction and oxidation of organic matter do not occur simultaneously, there could be an increase in the recombination of hole and electron that will decrease the photocatalysis reaction (Alhaji, et al., 2016). Thus, it is important to prevent recombination of hole and electron in order to achieve an efficient photocatalytic process. Heterogeneous catalysis can be considered a green technology because of two reasons. Firstly, it totally eliminates pollutants instead of changing the phase of the pollutants from one to another. Besides that, the process only requires ambient conditions and can fully break down organic pollutants into water and carbon dioxide (Zangeneh, et al., 2015).

2.3 Semiconductor Photocatalysts

Generally, a good catalyst should be mechanically and thermally stable, not easily poisoned and have a long lifetime (Unnikrishnan and Srinivas, 2016). For heterogeneous photocatalysis, many metal oxide semiconductors have been used as catalysts. Several examples of reported metal oxides used in photocatalysis are zinc oxide (ZnO), tungsten trioxide (WO₃), vanadium pentoxide (V₂O₅) and zirconium dioxide (ZrO₂) (Adhikari and Sarkar, 2015).

When considering the type of semiconductors to be used as photocatalyst, the band gap energy is crucial. The band gap energies of some common semiconductors on a potential scale (V) against the normal hydrogen electrode (NHE) are portrayed in Figure 2.2. This is because the band gap energy affects the recombination rate of holes and electrons and the amount of charge carriers that can be generated through absorption of light (Pawar and Lee, 2015). Besides, electron can only be promoted from the VB to the CB if the incoming photons have energy equal or larger than the band gap energy (Ragupathy, et al., 2015). In the visible light region, the spectra energy is between 2.43 eV to 3.2 eV (Pawar and Lee, 2015). This means that the effectiveness of the semiconductors in photocatalysis is affected by the choice of energy sources such as UV light or visible light and the band gap energy of the semiconductors.

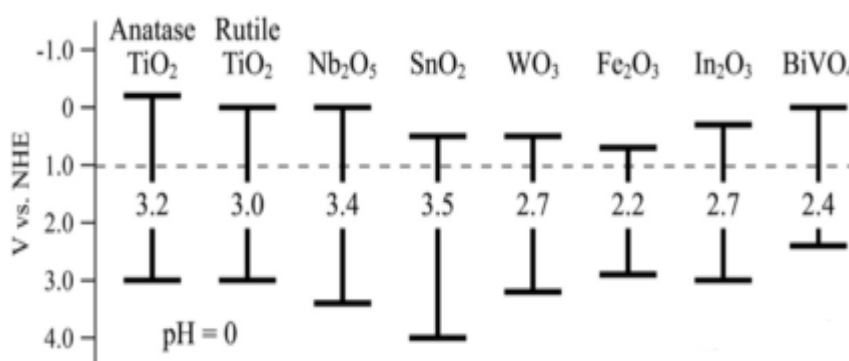


Figure 2.2: Band Gap Energies of Semiconductors on a Potential Scale (V) against the Normal Hydrogen Electrode (NHE) (Mano, et al., 2015)

Among many semiconductors, TiO₂ was found to have the most potential to be used in photocatalysis. This is because of its low energy requirement, great photocatalytic activity, high chemical stability, photostability, convenient obtainability, water insolubility, suitable flat band potential and ability to retard the formation of secondary by-products (Zangeneh, et al., 2015). TiO₂ can exist in three different crystal structures: anatase, brookite and rutile, as shown in Figure 2.3 (Liu, et al., 2013). It can be seen that both anatase and rutile structures have tetragonal crystallographic group while brookite has orthorhombic crystallographic group.

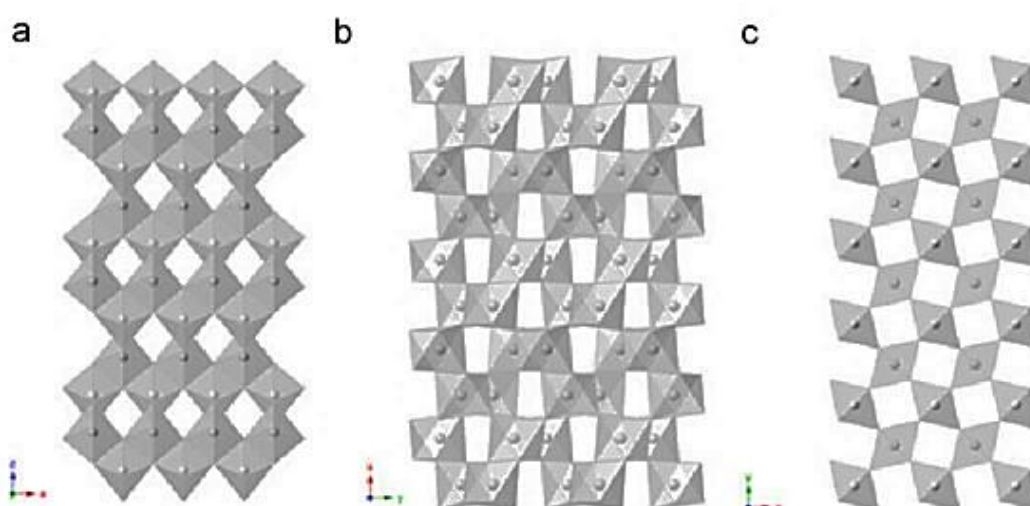


Figure 2.3: Structures of TiO₂, (a) Anatase, (b) Brookite, (c) Rutile (Liu, et al., 2013)

The anatase structure of TiO₂ is preferred over rutile structure because it is more efficient to be used in photocatalysis (Adhikari and Sarkar, 2015). There are a

few possible reasons for this. Firstly, the band gap energy of anatase is larger than rutile. This decreases the amount of light that can be absorbed but can also increase the valence band maximum to a higher energy level. This enhances the oxidation strength of electrons and helps in the transfer of electrons from TiO_2 to the adsorbed dye molecules. Besides that, the indirect band gap of anatase is higher than its direct band gap. Hence, the charge carrier lifetimes of anatase is longer and thus means the possibility of more occurrence of surface reactions (Luttrell, et al., 2014). Besides that, rutile is not that effective to be employed in photocatalysis because it requires a higher temperature, exhibits higher recombination of electron and hole and generally not preferred because of the lower electron lying at the CB edge (Zangeneh, et al., 2015).

The parameters that affect the photocatalytic activity of TiO_2 are crystallographic structure, surface area, size distribution, band gap, porosity and surface hydroxyl group density (Zangeneh, et al., 2015). TiO_2 can be used in wastewater treatment because of a few reasons. Firstly, the photocatalysis reaction can occur at room temperature. Secondly, TiO_2 produces intermediate products that can mineralize organic pollutants to less toxic products like carbon dioxide and water. Thirdly, the catalyst is not expensive and can be used in conjunction with various supports like stainless steel, glass, ACs, inorganic materials, fibres and sand which means high reusability. Lastly, photocatalysis in the presence of TiO_2 is able to generate extremely powerful electrons and holes that in turn produces superoxides that degrade many organic pollutants (Akpan and Hameed, 2009).

The problem with TiO_2 is that it has relatively large band gaps which are 3.2 eV for the anatase phase and 3.0 eV for the rutile phase. Hence, substantial photocatalytic activity can only be observed within a small percentage of incident solar irradiation which is less than 5 % (Ragupathy, et al., 2015). Visible light represents approximately 46 % of the energy from sunlight which is a more practical source (Cheng, et al., 2016). Various modifications have been proposed to improve the absorption of visible light in TiO_2 .

For example, two methods that had been proposed are doping and sensitization of TiO_2 (Zangeneh, et al., 2015). Both metals and non-metals can be doped with TiO_2 to increase its reactivity towards visible light. Several dopants are currently being investigated such as platinum (Pt), palladium (Pd), gold (Au), silver (Ag), cobalt (Co), iron (Fe), zinc (Zn), nickel (Ni) and nitrogen (N). The possible

mechanism of this modification involves the surface plasmon resonance of the metal particles being excited by visible light. This is followed by the promotion of the surface electron and interfacial electron exchange. Then, the metal disperses itself in the band gap of TiO_2 to create new energy levels. Finally, the deposited metals function as electron traps that will enhance the separation of the electron and hole (Diak, et al., 2015). However, metal doping is hindered by poor thermal stability while non-metal doping is not practical because of the much lower quantum efficiency under visible light as compared to UV light (Zangeneh, et al., 2015). As for sensitization of TiO_2 , dye which functions as the sensitizer adsorbs on the surface of TiO_2 , increasing the sensitivity of TiO_2 towards the visible light region. Next, the attached dye undergoes excitation by visible light. Lastly, the CB of TiO_2 is then injected with the electrons in the excited dye (Zangeneh, et al., 2015). When the dye absorbs light, it forms an excited triplet state in which following that, the absorbed energy is transferred to ground triplet state oxygen. This phenomenon produces singlet oxygen that is capable of degrading many organic pollutants, viruses and dormant bacteria (Yun, et al., 2017). In the past, organic dye photosensitisation of TiO_2 had been successful with the addition of phthalocyanine (Pc) complexes such as hybrid composites of TiO_2 and copper phthalocyanine and cobalt doped TiO_2 and phthalocyanine (Altin, et al., 2016).

On top of that, semiconductors are often combined together to obtain better properties and to compensate the individual backdrop (Adhikari and Sarkar, 2015). This surface modification is able to hinder the recombination of electron-hole and decrease the energy band gap that will enable more visible light to be absorbed. All these phenomena will enhance the photocatalytic activity. Several successful coupled semiconductors have been reported such as SnO_2/ZnO , TiO_2/MgO , ZnO/TiO_2 , WO_3/TiO_2 and CuO/TiO_2 (Saravanan, et al., 2013).

In addition to the problem of wide band gap, there are some other disadvantages of using powdered TiO_2 during the photocatalytic process. Firstly, it is hard to be separated from the liquid solution. Secondly, the catalyst could coagulate at high concentrations. Thirdly, the powder cannot be recycled easily (Martins, et al., 2017). Coagulation can cause less radiation from penetrating into the active centres because of reduced total surface area and hence decreasing the efficiency of the catalyst (Mahmoodi, et al., 2011). In that regard, many supports were proposed for TiO_2 including glass reactors, glass beads, glass mesh, glass wool, glass fabric,

microporous cellulosic membranes, monoliths, ceramic membranes, stainless steel and ACs (Mahmoodi, et al., 2011). Among all the supports, ACs have been given much attention. There are over 650 studies and 1000 patents about AC/TiO₂ composites in 2011 (Leary and Westwood, 2011). AC is the name given to carbon that is produced through treatment with oxidising gases or carbonisation of carbonaceous materials infused with dehydrating chemicals. Normally, AC has high porosity and large surface area (Rodriguez-Reinoso and Silvestre-Albero, 2016).

ACs were studied so intensively due to several reasons. One of them is the favourable properties of ACs. ACs possess very high surface area, robust and stable structures (Martins, et al., 2017). Other than being a good support for TiO₂, ACs also act as good adsorbents. They help to absorb pollutants towards the TiO₂ and also transport excited electrons away from the catalyst's surface, preventing accumulation of electrons. This will reduce the chances of electron-hole recombination and ensure holes and electrons have sufficient time to degrade the pollutants (Gao, et al., 2016). Despite that, there were some reports indicating that ACs prevented the transformation of TiO₂ from anatase to rutile but had little effect in reducing the coagulation of TiO₂ (Martins, et al., 2017). Besides that, it was suggested that TiO₂ nanoparticles seldom get attached successfully into the smaller pores of the AC and thus not fully realizing its potential (Leary and Westwood, 2011).

ACs can be obtained from carbonaceous or lignocellulosic materials (Mahmoodi, et al., 2011). Carbons can be extracted and then activated through chemical or physical means from biomass materials such as nutshell, coconut shell, almond shell, orange peel, rice husk, bamboo and many more (Sivakumar Natarajan, et al., 2016). Malaysia is the second largest producer of palm oil. Every year, there are 21.27 million metric tonnes of oil palm empty fruit bunch being produced (Ibrahim, et al., 2017). Rather than just burning the wastes away, they can actually be used to produce ACs. Besides that, it is cheaper to produce AC from biomass wastes and hence is a good alternative to commercial AC derived from coal that is expensive and cannot be used repeatedly (Hameed, et al., 2009).

2.4 Synthesis Method of AC/TiO₂ Photocatalyst

Xing, et al. (2016) reported that AC/TiO₂ composites were more efficient in photocatalytic degradation processes over normal TiO₂. Despite that, it was said that these composites are not used widely in treating wastewater because there are many

methods to produce them that leads to low reproducibility (Xing, et al., 2016). Over the past decade, many techniques had been suggested in the preparation of AC/TiO₂ photocatalyst. Some examples of the methods developed are sol-gel, metal-organic chemical vapour deposition (MOCVD) and hydrothermal. Among these methods, sol-gel is most popular because of its easy preparation steps and properly controlled morphology of TiO₂ on AC (Xing, et al., 2016).

According to Danks, et al. (2016), sol-gel can be ceramic or inorganic polymer and is prepared from the transformation from liquid precursors to a sol that subsequently forms a network structure named 'gel'. Most of these sol-gels are formed through the condensation and hydrolysis of metal alkoxide precursors (Danks, et al., 2016). Some of the noticeable advantages of the sol-gel method are the milder preparation conditions, effective control of the shape, particle size and properties of the fabricated material, flexibility in the control of material structure and good mixing for multicomponent systems (Tseng, et al., 2010). The last two benefits might be useful in the preparation of composite like AC/TiO₂. In the past, researchers had successfully produced AC/TiO₂ composite by the sol-gel method from different precursors. For example, Xing, et al. (2016) used tetrabutyl titanate while Singh, et al. (2016) used titanium tetra-isopropoxide as precursor. In both cases, after the TiO₂ sol was formed, it was mixed with AC, solidified and calcined to form the AC/TiO₂ composite.

The second preparation method is MOCVD which is a variant of the conventional chemical vapour deposition method. According to Li Puma, et al. (2008), this method involves the use of an inert gas such as nitrogen to carry the vaporised precursor to the activated carbon support. The flow pressure needs to be well-controlled to avoid uneven film uniformity. This technique can be used to produce metal-oxide-containing composites at milder conditions due to the use of metallo-organic precursors that are generally very volatile. Besides that, the steps are generally simpler because activation and reduction can occur simultaneously in the reactor (Li Puma, et al., 2008). TiO₂ supported on almond shell-derived activated carbon had been successfully synthesized using this method (Omri, et al., 2014).

The last method to produce AC/TiO₂ is hydrothermal. According to Suib (2013), this method requires high temperature and pressure. It is useful in creating crystalline phases that have low stability at the melting point and high vapour pressure near the melting point. Besides that, the hydrothermal method allows the

production of big and high-quality crystals with well-controlled composition (Suib, 2013). The hydrothermal method had been proven successful in producing AC/TiO₂ as reported by Meng, et al. (2014) and Sivakumar Natarajan, et al. (2016).

2.5 Characterisation Study

Characterisation of the synthesised photocatalysts is vital in the development of any new catalyst because it provides valuable information about the chemical properties and surface morphology of the catalysts. A well-executed characterisation will allow reasoning to be formed on the effectiveness or lack of performance of the catalysts. Some of the characterisation tools have been used for characterisation of catalyst. For instance, X-ray diffraction (XRD) is used to study the crystal phase composition and crystallite sizes of the catalysts. Scanning electron microscopy (SEM) is used to study the surface morphology and elemental composition of the catalyst. Fourier transformed infrared (FT-IR) spectroscopy is used to study the surface functional groups inside the catalysts. Thermogravimetric analysis (TGA) is used to study the thermal stability of the catalyst and lastly nitrogen adsorption and desorption isotherms to find out the Brunauer-Emmett-Teller (BET) surface area of the catalysts.

In XRD analysis, crystal structures of TiO₂ can be found out. It is desirable to know whether anatase or rutile phase is predominant in the TiO₂ and the effect that AC has on the structure. Besides that, the average crystallite sizes can also be easily determined. Smaller crystallite sizes correspond to higher surface areas which is important as more TiO₂ can be attached on the AC. In addition, the transformation of anatase to rutile phase could also be prevented if the AC matrix surface area was large (Martins, et al., 2017). To calculate the average crystal size, the Scherrer's equation can be used, as shown in Equation 2.9 (Singh, et al., 2016). Results obtained by Martins, et al. (2017) indicated that AC/TiO₂ had smaller crystal size than TiO₂. The smaller crystal sizes in AC/TiO₂ was due to the presence of AC decomposition products in the TiO₂ crystal structure. Apart from that, they also discovered that no rutile phase in AC/TiO₂ because of the low pyrolysis temperature (500 °C) used in which anatase was still stable. It was said that transformation to rutile phase began around 700 °C. (Martins, et al., 2017).

$$D = \frac{K\lambda}{\beta \cos\theta} \quad (2.9)$$

where

K = Scherrer constant

D = average crystalline size

λ = X-ray wavelength

β = the peak width of half maximum

θ = Bragg diffraction angle

SEM is useful to look deeper into the surface morphology of the catalysts. Study performed by Sivakumar Natarajan, et al. (2016) showed that the activated carbon had oval shaped pores and was arranged to form thin layers of ladder. In addition, it was also found that there was good dispersion of TiO₂ nanoparticles on activated carbon fibres up to a certain TiO₂ concentration (0.35 mol/L). The amount of attached TiO₂ would decrease as a result of clustering of TiO₂ into larger sizes (Meng, et al., 2014). EDX coupled with SEM can be used to determine the elemental composition of the catalysts (Mohammadzadeh, et al., 2015).

FT-IR can be used to obtain information about the functional groups present in the catalysts. For example, hydroxyl group can be determined by this method. In a research conducted by Ragupathy, et al. (2015), they found that sharp peaks in the FT-IR spectra corresponded to various functional groups. There was a broad band between 3000-3700 cm⁻¹ because of the O-H stretching mode of the hydroxyl group. This observation was corroborated by Singh, et al. (2016) who also suggested that there was a modification in the acid-base characteristics of the hydroxyl group. As previously mentioned, hydroxyl radicals are important due to their ability to interact with the holes formed in the photocatalytic process.

TGA can be used to examine the thermal stability of a material and the percentage of volatile components inside the material. The changes in weight that occurs in the material as it is being heated is the subject of interest. The analysis is usually performed either in air or inert atmosphere. The weight is normally plotted against temperature (Liu, et al., 2014). Study conducted by Muniandy, et al. (2016) employed TGA to determine the percentage of carbon in modified TiO₂. It was found

that AC/TiO₂ composite consisted of mainly water molecules and carbon. There was no significant weight loss observed for pure TiO₂ (Muniandy, et al., 2016).

Nitrogen adsorption and desorption isotherms can be used to determine properties such as pore size distribution and BET surface area. Based on McCusker, et al. (2003), pore sizes smaller than 2 nanometres are known as micropores while those between 2 and 50 nanometres are mesopores. Previous research had shown that AC/TiO₂ had mesoporous structures and had distributions between 4 to 10 nanometres. This revelation indicated that the composite catalyst is suitable for photocatalytic degradation process because such structures enable efficient transport of charged carriers formed in the photocatalytic process (Martins, et al., 2017).

2.6 Kinetics of Photocatalytic Degradation

The photocatalytic activity of the AC/TiO₂ should be studied. Before the suitable kinetic models can be proposed, the reaction kinetic order needs to be determined first. Various experiments have been carried out over the years to understand the kinetics of photocatalytic oxidation. Some researchers had found that modelling the photocatalytic degradation using pseudo first-order kinetic equation was sufficient and fitted the Langmuir-Hinshelwood dynamic model as shown in Equation 2.10 (Chen, et al., 2016; Konstantinou and Albanis, 2004). This model means that the reaction rate is dependent on the dye concentration.

$$r = \frac{dC}{dt} = \frac{kKC}{1 + KC} \quad (2.10)$$

where

r = oxidation rate of the dye, $\frac{\text{mg}}{\text{L}\cdot\text{min}}$

C = concentration of the dye at any time, $\frac{\text{mg}}{\text{L}}$

K = adsorption coefficient of the dye, $\frac{\text{mg}}{\text{L}}$

k = reaction rate constant, $\frac{\text{mg}}{\text{L}\cdot\text{min}}$

t = illumination time, min

If the initial dye concentration, C_0 is very small, the equation can be simplified to an apparent first-order equation, as shown in Equation 2.11.

$$\ln\left(\frac{C_0}{C}\right) = kKt = k_{app}t \quad (2.11)$$

Plotting $\ln\left(\frac{C_0}{C}\right)$ against time will produce a straight line. The gradient of the best-fit line will be the apparent first-order rate constant, k_{app} . The rate constant is a direct indication on the speed and efficiency of the photocatalytic degradation process. The expressions mentioned are accurate in four possible conditions mainly reaction occurring between two adsorbed substances, reaction happening between a radical in solution and an adsorbed substrate molecule, reaction occurring between a radical linked to the surface and a substrate molecule in the solution and finally reaction occurring with both species in the solution (Konstantinou and Albanis, 2004). In this research, pseudo zero and second-order kinetic equations will also be tested to determine the suitability of the photocatalytic degradation process. Pseudo zero-order kinetic means that the active sites are saturated by organic molecules (Asenjo, et al., 2013). It generally means the dye degradation rate is independent of the dye concentration. Meanwhile, pseudo second-order indicates that the reaction rate is limited by surface adsorption involving chemisorption (Robati, 2013). Study conducted by Ma, et al. (2017) showed that pseudo second-order kinetic was obtained at higher concentrations of Congo Red while pseudo first-order kinetic was observed at lower concentrations.

2.7 Parameters Influencing the Photocatalytic Degradation

Various experiments had been carried out on TiO₂-based photocatalysts or involving different semiconductors in the past for the purpose of degrading pollutants such as organic dye. It was established that there were a few parameters that would affect the rate of photodegradation. These parameters included the effect of various types of organic dyes, weight ratio of AC/TiO₂ composite, catalyst loading, solution pH, initial dye concentration and solution temperature.

2.7.1 Effect of Various Types of Organic Dyes

It was noted that the same photocatalyst can have different performance on different types of organic dyes. According to Liu, et al. (2017), the degradation rates for Rhodamine B and Methyl Orange were 97.8 % and 5.6 % respectively after irradiation for 90 minutes. This was due to the different structure of the dyes. It was

discovered that the catalyst had nanomella petals growing in the ab plane that enhanced the adsorption of Rhodamine B because it had the $N(Et)_2$ groups. In contrast, this functional group was absent in Methyl Orange. Besides that, it was also found that the chemical bonds present in the dye were the main factor for differences in degradation rates. The degradation of Rhodamine B and Methyl Orange involved the breaking of C-C and C-N bonds respectively. It was noted that the bond energy of C-N bonds was larger than that of C-C bonds. Hence, the superoxide anions and hydroxyl radicals could not break the C-N bonds as easily (Liu, et al., 2017).

2.7.2 Effect of AC/TiO₂ Composite at Different Weight Ratio

The weight ratio of AC/TiO₂ affected the photocatalytic degradation efficiency. Study carried out by Sivakumar Natarajan, et al. (2016) had seen tremendous increase in photocatalytic performance of Rhodamine B when AC loading was increased. This was due to three reasons. Firstly, the increased in AC loading led to higher surface area for adsorption of TiO₂ which in turn enhanced the photocatalytic degradation process. Secondly, there was a decrease in band gap energy with increased AC loading which allowed more energy to be absorbed by the TiO₂ particles which subsequently generated more hydroxyl radicals. Lastly, the increased AC loading also further inhibited the recombination of electron-hole pair (Sivakumar Natarajan, et al., 2016). It was also observed by that the removal of dye solution is contributed by adsorption of dye molecules by the carbon and photocatalytic decomposition by TiO₂ (Chen, et al., 2007).

2.7.3 Effect of Catalyst Loading

The amount of catalyst loaded is vital in the photodegradation process. Based on Ahmed, et al. (2010), the photodegradation rate would increase with the amount of catalyst loading up to a certain point and then started to decrease because of screening effect and light scattering. This means that light could not be distributed evenly resulting in lower reaction rates. This was also confirmed by Ragupathy, et al. (2015) as they discovered that increasing catalyst loading resulted in higher degradation rate. They found out that the rate of degradation increased only up to a loading of 0.2 g/L and no further increase was seen with higher catalyst loading. It was reasoned that the increase in adsorption sites and number of photons attaching to the sites gave rise to the observation. Besides that, it was also asserted that the

increase in catalyst loading resulted in the enhanced availability of catalyst surface area for the free radicals production which was directly proportional to the photocatalytic degradation efficiency (Nethaji, et al., 2017). In addition, aggregation of the catalyst particles was also pointed out as a reason for the decrease in reaction rate beyond the optimum catalyst loading (Ng, et al., 2016). This could be contributed to the screening effect. Hence, the optimal amount of catalyst loading should be determined for better photocatalytic degradation performance.

2.7.4 Effect of Solution pH

Most semiconductor oxides exhibit amphoteric behaviour and can affect the surface charge properties of the catalyst (Mohammadzadeh, et al., 2015). Amphoteric means that they can react as acids or bases. The reason behind why solution pH is important in photocatalysis is because of the electrostatic interactions that can occur between the catalyst and dye. The pH where the surface of an oxide is uncharged is called the zero-point charge. In TiO₂, the zero-point charge is somewhere between pH 2.9 to pH 7 (Liu, et al., 2011). When the pH of the solution is below this point, the catalyst is positively-charged and above that negatively-charged (Gomathi Devi and Mohan Reddy, 2010). Mohammadzadeh, et al. (2015) stated that the dye can be positively or negatively charged depending on whether the pH is higher than the acid dissociation constant or not. If it is higher, then it is negatively-charged. If at the right pH, the dye and catalyst are of different charges, there will be an electrostatic attraction between them leading to more dye molecules being adsorbed on the surface to be degraded. Thus, there will be an increase in the photocatalytic activity (Mohammadzadeh, et al., 2015). From here, it was understood that solution pH is an important parameter that must be controlled for effective photocatalytic degradation.

2.7.5 Effect of Initial Dye Concentration

The adsorption of dye on the surface of the catalyst is very much linked to the initial dye concentration. When the initial dye concentration increases, the percentage of dye removal will decrease. This is because at high concentrations, the dye molecules might absorb a significant portion of the light source and not the catalyst due to the decrease in path length of photon penetrating into the solution (Sobana, et al., 2013). Besides that, high concentrations will encourage the adsorption sites to fill up quickly and become saturated. Hence, there will be less available for more dye

molecules to be adsorbed which will lead to a decrease in the photodegradation activity. Nevertheless, it was also theorized that the capacity of the adsorbent might actually increase with dye concentrations because of the high driving force for mass transfer (Yagub, et al., 2014). A study performed by Chen, et al. (2016) also proved the above points. They found out that the degradation rate of cefradine decreased beyond 20.0 mg/L which can be assumed to be the optimum initial concentration. Thus, it can be said that there is an optimal initial dye concentration in which photocatalytic degradation is most efficient.

2.7.6 Effect of Solution Temperature

Generally, an increase in solution temperature will result in an increase of degradation rate. The reaction rate is temperature dependent and can be expressed with the Arrhenius equation as shown in Equation 2.12 (Omri, et al., 2014). When solution temperature increases, there is an increase the movement of the dye molecules towards the external boundary layer allowing more dyes to be attached to the catalyst surface and also the inner pores (Saini, et al., 2017). Besides that, alteration of the temperature will also result in changes in the equilibrium capacity of the catalyst for dye molecules (Bazrafshan, et al., 2015). In addition, depending on whether the reaction is endothermic or exothermic, increasing temperature will affect the degradation rate differently. If the rate increases, it is endothermic and if it decreases, it is exothermic (Yagub, et al., 2014). A study performed by Alhaji, et al. (2016) on the degradation of palm oil mill effluents indicated that photocatalytic degradation rate increased up to a high of 80 °C and decreased subsequently. This was attributed to the increase of hole-electrons recombination which led to a decrease in adsorption of organic molecules on the TiO₂ surface. From all the observations, an optimum temperature exists in which the photocatalytic degradation rate is at its maximum.

$$k = A \exp\left(-\frac{E_a}{RT}\right) \quad (2.12)$$

where

k = reaction rate constant, min⁻¹

A = pre-exponential constant, min⁻¹

E_a = activation energy, J/mol

R = gas constant, 8.314 J/mol·K

T = temperature, K

CHAPTER 3

METHODOLOGY AND WORK PLAN

3.1 Materials and Chemicals

The list of chemical reagents used in the preparation of the AC/TiO₂ photocatalyst and their respective specifications and sources are shown in Table 3.1. From the table, Potassium Hydroxide (KOH) and n-Hexane were used for the preparation of AC while Isopropanol and Titanium (IV) Isopropoxide (TTIP) were used to synthesize the AC/TiO₂ photocatalyst. Titanium Dioxide was also utilised as a photocatalyst in the research. The different types of dyes used for the parameter studies were also listed.

Table 3.1: List of Chemical Used and its Specifications

Chemical Reagent	Grade	Supplier	Usage
Isopropanol	Analysis	Merck	Solvent for AC/TiO ₂ synthesis
n-Hexane	Analysis	Merck	Solvent for oil extraction
KOH	Analysis	Chemsoln	Reagent for modification and activation of AC
TTIP, 97 %	Analysis	Sigma-Aldrich	Titanium source for AC/TiO ₂ synthesis
TiO ₂	Analytical Reagent (A.R.)	R & M Chemicals	Photocatalyst
Malachite Green	99 % Purity	Fisher Scientific	Model pollutant
Reactive Blue 4	35 % Purity	R & M Chemicals	Model pollutant
Congo Red	40 % Purity	R & M Chemicals	Model pollutant
Rhodamine B	95 % Purity	Sigma-Aldrich	Model pollutant
Methylene Blue	82 % Purity	R & M Chemicals	Model pollutant

The chemical properties such as the molecular formula, molecular weight, maximum absorption wavelength and molecular structure of the model pollutants used to investigate the photodegradation activity are stated in Table 3.2.

Table 3.2: The Chemical Properties of Model Pollutant Used in Research (Kamalakkannan, et al., 2015)

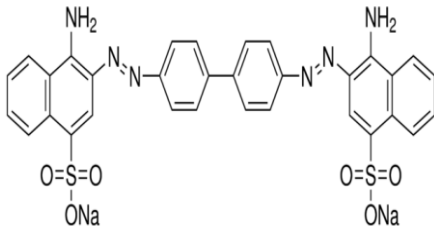
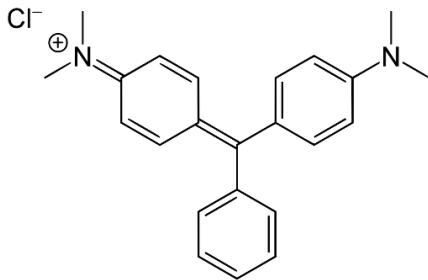
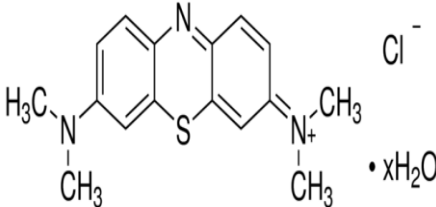
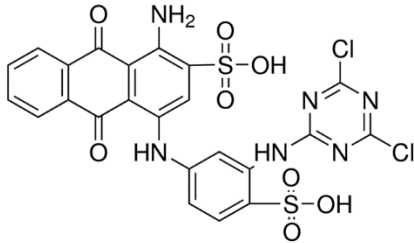
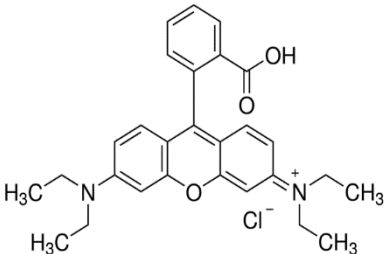
Dye	Molecular Formula	Molecular Weight (g/mol)	Maximum Absorption Wavelength, λ_{max} (nm)	Molecular Structure
Congo Red	$\text{C}_{32}\text{H}_{22}\text{N}_6\text{Na}_2\text{O}_6\text{S}_2$	696.66	498	
Malachite Green	$\text{C}_{23}\text{H}_{25}\text{ClN}_2$	364.911	619	

Table 3.2: Continued

Dye	Molecular Formula	Molecular Weight (g/mol)	Maximum Absorption Wavelength, λ_{\max} (nm)	Molecular Structure
Methylene Blue	$C_{16}H_{18}ClN_3S \cdot xH_2O$	319.85	665	
Reactive Blue 4	$C_{23}H_{14}Cl_2N_6O_8S_2$	637.419	595	
Rhodamine B	$C_{28}H_{31}ClN_2O_3$	479.01	555	

3.2 Equipment

Table 3.3 lists out the major equipment used for this research with their respective functions. The programmable furnace was used to calcine the AC and AC/TiO₂. Analytical equipment such as SEM-EDX, XRD, simultaneous thermal analyser, FT-IR spectrometer and sorptomatic surface area analyser were used for the characterisation study. Analysis of liquid samples was performed using UV-Vis spectrophotometer. COD reactor was utilised to heat sample with COD digestion reagent vials. Lastly, hot plate magnetic stirrer was utilised to ensure homogenous mixing of the catalyst and dye solution as well as heating of dye solution.

3.3 Overall Flowchart of Research

Figure 3.1 depicts the flowchart for overall research activities. Firstly, the activated carbon was prepared using empty fruit bunch fibres by calcination. Then, the activated carbon was impregnated with TiO₂ using the sol-gel synthesis method. The resultant composite was then characterised using XRD, SEM-EDX, FT-IR spectroscopy, TGA and BET analysis. Next, several parameter studies were performed on Malachite Green dye by changing the weight ratio of AC/TiO₂ composite, catalyst loading, initial dye concentration, solution temperature and types of organic dyes. The liquid sample was then analysed using the UV-Vis spectrophotometer and COD analysis. The reusability of the catalyst was also examined. Finally, kinetic studies were performed on the photodegradation process.

3.4 Experimental Setup

The experimental setup for the photocatalytic degradation experiment is shown in Figure 3.2. A fluorescent light bulb was used as the source of visible light. In order to fix the light bulb in place, the light bulb was plugged to a power socket adaptor secured by the clamp of the retort stand. To ensure homogenous mixing of the dye solution and photocatalyst, a hot plate magnetic stirrer was used together with a magnetic stir bar placed in the beaker. Lastly, the beaker was covered with aluminium foil on the sides to ensure that the light source was coming only from the top.

Table 3.3: List of Equipment Used and its Respective Function

Equipment	Model	Function
Fourier Transform Infrared Spectrometer	Nicolet IS10	Comparison of active surface functional groups of photocatalyst
Programmable Furnace	Wise Therm FP-03	Calcination of AC and AC/TiO ₂
Scanning Electron Microscope- Energy Dispersive X-Ray	Hitachi S-3400 N	Morphology and elemental analysis
Simultaneous Thermal Analyzer	Perkin Elmer STA8000	Thermal stability analysis
Sorptomatic Surface Area Analyzer	Thermo Scientific SO1900	Specific surface area analysis
UV- Vis Spectrophotometer	Jenway 6320D	Measurement of dye concentration
X-Ray Diffractometer	Shimadzu XRD-6000	Crystal phases and crystallite sizes analysis
COD Reactor	Hach DRB200	Heating of COD vials
Hot Plate Magnetic Stirrer	IKA 362001 RET Basic	Mixing and heating of catalyst in dye solution

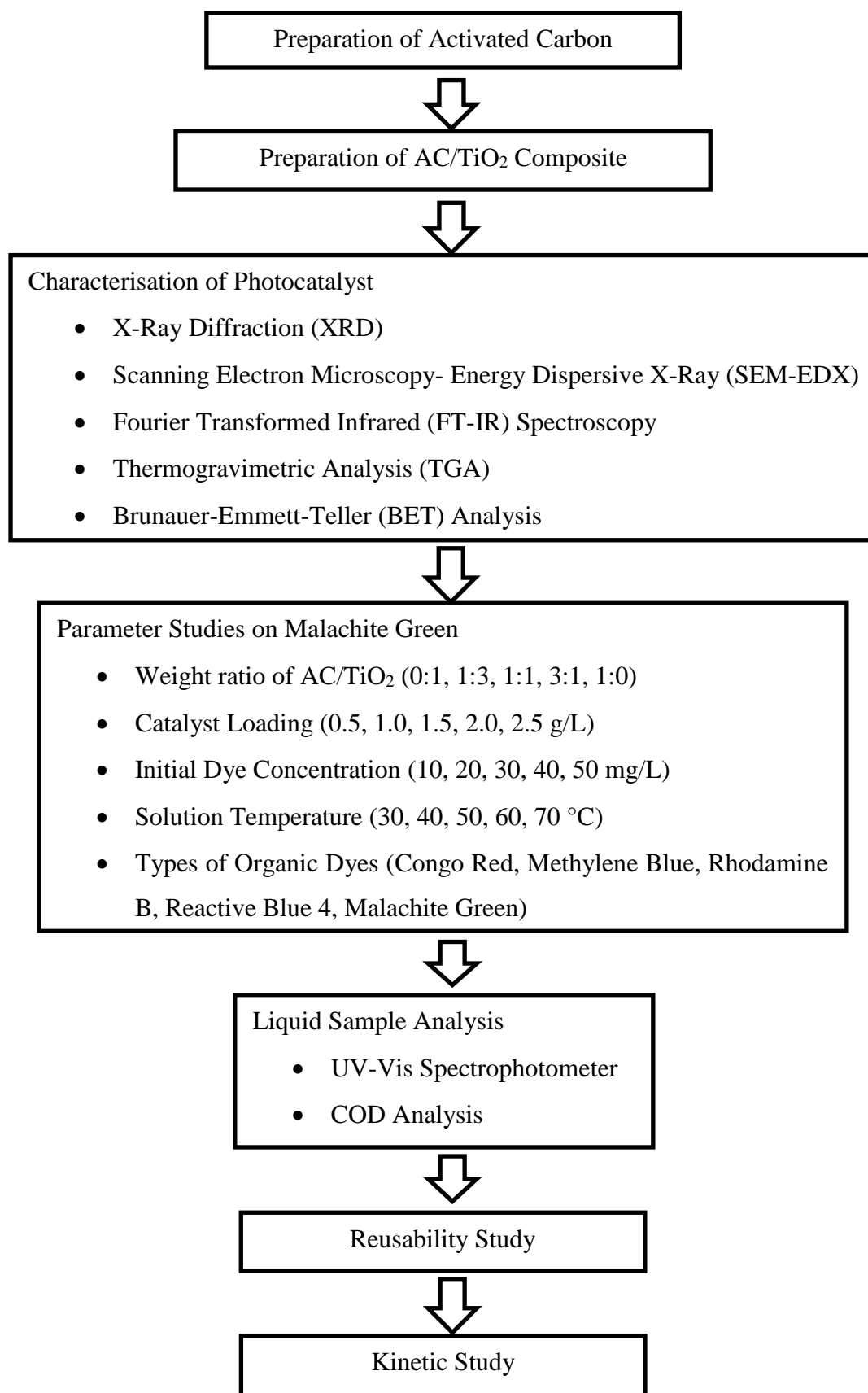


Figure 3.1: Flowchart of Overall Research Activities

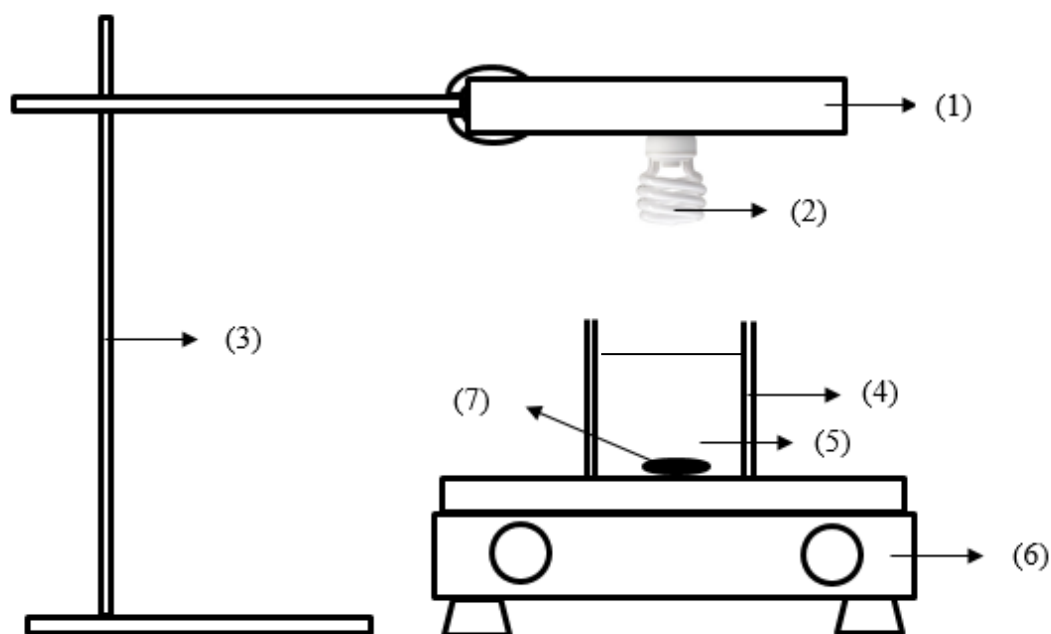


Figure 3.2: Schematic Diagram of the Experimental Setup (1) Power Socket Adaptor, (2) Fluorescent Bulb, (3) Retort Stand with Clamp, (4) Aluminium Foil, (5) Beaker, (6) Hot Plate Magnetic Stirrer, (7) Magnetic Stir Bar

3.5 Preparation of Catalyst

The preparation of the AC/TiO₂ composite was performed in two steps. First, the carbon was derived from a suitable biomass such as empty fruit bunch fibres and then activated. Second, the activated carbon is used with a suitable titanium precursor to form the composite through the sol-gel method.

3.5.1 Preparation of Activated Carbon

The activated carbon was prepared using a modified version of the method outlined by Ragupathy, et al. (2015). Empty fruit bunch fibres were used as the carbon source. The fibres were first cut into smaller pieces. Then, the fibres were soaked in n-Hexane for two hours to remove the residue oil from the EFB fibres. After that, the fibres were washed with hot distilled water over a filter funnel for three times. Then, the fibres were dried in the oven at 80 °C until dry. Next, the fibres were soaked in 1.0 M KOH solution for 2 hours to modify and activate the empty fruit bunch fibres. The fibres were then washed with distilled water for three times over a filter funnel and were placed in the oven to dry at 90 °C overnight. The dried fibres were then

calcined at 650 °C for 120 minutes with the ramp rate of 20 °C/min. After cooling to ambient temperature, the obtained sample was washed with distilled water for three times. Then, the sample was filtered and dried in the oven at 90 °C overnight.

3.5.2 Preparation of AC/TiO₂ Composite

The synthesis of AC/TiO₂ composite material was performed using the sol-gel synthesis method (Martins, et al., 2017). 10 mL of TTIP was diluted in 90 mL of isopropanol. The solution was stirred for 5 minutes at room temperature before 2.8 g of AC was added and stirred. Then, 30 mL of water was added dropwise into the mixture and stirred vigorously for two hours to obtain a homogeneous gel. The gel was then dried at 100 °C for 2 hours to evaporate the water and organic residues and then grounded using a mortar to avoid agglomeration. Next, the gel was calcined at 500 °C for 2 hours. The resulting material was washed with distilled water several times until the supernatant looks transparent. Then, they were dried in the oven at 100 °C overnight. The obtained material was labelled as AC/TiO₂.

3.6 Characterisation of Photocatalysts

The crystallinity, thermal stability, functional groups, surface morphology and specific surface area of the three samples consisting of AC, TiO₂ and AC/TiO₂ catalysts need to be characterised in order to obtain an in-depth understanding of their properties. The elemental compositions and chemical properties of the catalysts can be determined. Reasoning can also be formed based on the underlying knowledge of their properties. In this research, the catalysts were characterised using XRD, SEM-EDX, FT-IR spectroscopy, TGA and BET analysis.

3.6.1 XRD

The crystal phases and crystallite sizes of the three samples were analysed using the X-ray diffractometer model XRD-6000 supplied by Shimadzu. X-rays were first focused on the fixed sample and then subsequently diffracted. The changes in the diffracted X-ray intensities were measured, recorded and plotted against the rotation angles of the sample. The obtained X-ray diffraction pattern was analysed qualitatively on the basis of peak height or peak area. Through these, the particle diameters and degree of crystallization were calculated.

3.6.2 SEM-EDX

The surface morphology and elemental composition of the three samples were determined using a scanning electron microscope model S-3400N supplied by Hitachi. The sample was first mounted onto an appropriately sized pin stub which was then inserted into a brass carrier. Then, the sample height was measured with respect to the standard height using the supplied height measurement tool. The overall specimen size was also noted. The SEM was then started by turning on the beam. The image was then viewed and analysed. By using EDX together with SEM, the elemental composition of the catalysts was determined.

3.6.3 FT-IR Spectroscopy

Comparisons between the active surface functional groups in the three samples were performed using the FT-IR Spectrometer model Nicolet IS10 supplied by ThermoFisher Scientific. The sampling method used here was attenuated total reflectance (ATR). The FT-IR spectra were recorded in the spectral range of 4000-400 cm^{-1} at a resolution of 4 cm^{-1} and 254 scans. The spectra were then compared with the one available in the database using the search function.

3.6.4 TGA

The thermal stability and decomposition of the samples were analysed using Simultaneous Thermal Analyzer model STA8000 provided by Perkin Elmer. The sample was subjected to heating from 30 to 1000 °C under air atmosphere with a heating rate of 10 °C/min under air flow. The weight loss was then plotted against temperature to determine the percentage of volatile components in the samples.

3.6.5 BET Analysis

The specific surface area of the samples was determined by measuring the nitrogen adsorption-desorption isotherm at 77 K using the Sorptomatic Surface Area Analyzer model SO1900 provided by Thermo Scientific. Prior to the BET analysis, the samples were degassed at 200 °C overnight before nitrogen adsorption-desorption measurements.

3.7 Parameter Studies

The photodegradation activity of Malachite Green was studied by varying the operating parameters such as the weight ratio of AC/TiO₂ (0:1-1:0), amount of catalyst loading (0.5-2.5 g/L), initial dye concentration (10-50 mg/L), solution temperature (30-70 °C) and various types of organic dyes.

3.7.1 Effect of Various Types of Organic Dyes

In order to study the effect of various types of organic dyes on the degradation rate, five types of organic dyes were used. They were Congo Red, Methylene Blue, Rhodamine B, Reactive Blue 4 and Malachite Green. 2.5 g/L of AC/TiO₂ catalyst at weight ratio 3:1 was added to 100 mL of 10 mg/L Malachite Green in a beaker. The solution temperature was set to 50 °C. Then, the sample was left in the dark for 30 minutes to allow complete adsorption at equilibrium. After that, the sample was irradiated under visible light. About 5 mL of the sample was collected every 30 seconds for 7.5 minutes. The sample was then filtered to separate the photocatalyst from the dye solution and analysed using the UV-Vis spectrophotometer. The process was repeated for the other 4 organic dyes, keeping all other parameters at constant values. Malachite Green was utilised for the subsequent parameter study because it recorded the highest degradation efficiency.

3.7.2 Effect of AC/TiO₂ Composite at Different Weight Ratio

The effect of AC/TiO₂ composite at different weight ratio was studied by varying the ratio at 0:1, 1:3, 1:1, 3:1 and 1:0. Firstly, 100 mL of 10 mg/L Malachite Green was filled into a beaker together with 2.5 g/L of AC/TiO₂ composite at weight ratio 3:1 under magnetic stirring. The solution temperature was fixed at a room temperature of 30 °C. The sample was then left in the dark for 30 minutes to allow the complete adsorption at equilibrium. After that, the sample was irradiated under visible light. About 5 mL of the sample was collected every 2 minutes for 30 minutes. The sample was then filtered to separate the photocatalyst from the dye solution and analysed using the UV-Vis spectrophotometer. The process was repeated for the other 4 sets, keeping all other parameters at constant values. AC/TiO₂ catalyst at weight ratio 3:1 was utilised for the subsequent parameter study.

3.7.3 Effect of Catalyst Loading

The effect of the catalyst loading on the photocatalytic degradation rate was examined by setting the catalyst loading at 0.5, 1.0, 1.5, 2.0 and 2.5 g/L. Firstly, 100 mL of 10 mg/L Malachite Green was filled into a beaker together with 0.5 g/L of AC/TiO₂ composite at weight ratio 3:1 under magnetic stirring. The solution temperature was fixed at a room temperature of 30 °C. The sample was then left in the dark for 30 minutes to allow the complete adsorption at equilibrium. After that, the sample was irradiated under visible light. About 5 mL of the sample was collected every 2 minutes for 30 minutes. The sample was then filtered to separate the photocatalyst from the dye solution and analysed using the UV-Vis spectrophotometer. The process was repeated for the other 4 sets, keeping all other parameters at constant values. AC/TiO₂ catalyst at weight ratio 3:1 with optimum loading of 2.5 g/L was utilised for the subsequent parameter study.

3.7.4 Effect of Initial Dye Concentration

The effect of initial dye concentration on the degradation rate of Malachite Green was studied by varying the initial dye concentration to 10, 20, 30, 40 and 50 mg/L. Firstly, 100 mL of 10 mg/L Malachite Green was filled into a beaker together with 2.5 g/L of AC/TiO₂ catalyst at weight ratio 3:1 under magnetic stirring. The solution temperature was fixed at a room temperature of 30 °C. The sample was then left in the dark for 30 minutes to allow the complete adsorption at equilibrium. After that, the sample was irradiated under visible light. About 5 mL of the sample was collected every 2 minutes for 30 minutes. The sample was then filtered to separate the photocatalyst from the dye solution and analysed using the UV-Vis spectrophotometer. The process was repeated for the other 4 concentration values, keeping all other parameters at constant values. Malachite Green solution of 10 mg/L was used for the subsequent parameter study.

3.7.5 Effect of Solution Temperature

To study the effect of solution temperature on the degradation rate, the solution temperature was varied to 30, 40, 50, 60 and 70 °C. Firstly, 100 mL of 10 mg/L Malachite Green was filled into a beaker together with 2.5 g/L of AC/TiO₂ catalyst at weight ratio 3:1 under magnetic stirring. The solution temperature was fixed at a room temperature of 30 °C. The sample was then left in the dark for 30 minutes to

allow the complete adsorption at equilibrium. After that, the sample was irradiated under visible light. About 5 mL of the sample was collected every 30 seconds for 7.5 minutes. The sample was then filtered to separate the photocatalyst from the dye solution and analysed using the UV-Vis spectrophotometer. The process was repeated for the other 4 temperature values, keeping all other parameters at constant values. The optimum solution temperature was 50 °C.

3.8 Reusability Study

In order to study the reusability of the catalyst, 2.5 g/L of AC/TiO₂ catalyst at weight ratio 3:1 was added to 100 mL of 10 mg/L Malachite Green in a beaker. The solution temperature was set to 50 °C. Then, the sample was left in the dark for 30 minutes to allow complete adsorption at equilibrium. After that, the sample was irradiated under visible light. About 5 mL of the sample was collected every 2 minutes for 30 minutes. The sample was then filtered to separate the photocatalyst from the dye solution and analysed using the UV-Vis spectrophotometer. Then, the catalyst was retrieved and rinsed thoroughly with distilled water for three times. It was then dried in the oven at 90 °C until dry. The catalyst was then used in the subsequent cycle involving the same conditions above.

3.9 Kinetic Study

Three kinetic expressions were tested to determine the suitability model of the photocatalytic degradation process. These are pseudo zero-order, pseudo first-order and pseudo second-order kinetic expressions. The reactions are shown in Equations 3.1 to 3.3. By measuring the dye concentration at regular intervals, dye concentration can be plotted against time. For pseudo zero-order, $C_0 - C_t$ was plotted against t , $\ln(C_0/C_t)$ against t for pseudo first-order and $1/C_t - 1/C_0$ for pseudo second-order. The model that produced a straight line was chosen as the most suitable model for the photocatalytic degradation process.

Zero-order:

$$C_t = C_0 - k_0 t \quad (3.1)$$

First-order:

$$\ln C_t = \ln C_0 - k_1 t \quad (3.2)$$

Second-order:

$$\frac{1}{C_t} = \frac{1}{C_0} + k_2 t \quad (3.3)$$

where

C_0 = initial dye concentration, $\frac{\text{mg}}{\text{L}}$

C_t = dye concentration at time t , $\frac{\text{mg}}{\text{L}}$

k_0 = apparent pseudo zero-order rate constant, $\frac{\text{mg}}{\text{L}\cdot\text{min}}$

k_1 = apparent pseudo first-order rate constant, min^{-1}

k_2 = apparent pseudo second-order rate constant, $\frac{\text{L}}{\text{mg}\cdot\text{min}}$

3.10 Liquid Sample Analysis

The concentration of the dye at every interval was determined to study the percentage degradation of Malachite Green over time. The absorbance of the dye was measured at the maximum absorption wavelength, 619 nm by utilizing the UV-Vis spectrophotometer. Based on Beer-Lambert Law, the absorbance of a solution is directly proportional to the concentration of the solution. Hence, a calibration curve was drawn based on the absorbance value. The photocatalytic degradation efficiency was calculated using Equation 3.4.

$$\text{Degradation Percentage} = \frac{C_0 - C_t}{C_0} \times 100\% \quad (3.4)$$

where

C_0 = initial concentration of dye, $\frac{\text{mg}}{\text{L}}$

C_t = concentration of dye after irradiation at time t , $\frac{\text{mg}}{\text{L}}$

COD analysis was performed to determine the quantity of organic compounds in the sample. This analysis is commonly used to identify the quality of water. It measures the consumption of oxygen by water during the oxidation of organic compounds by a strong oxidizing agent to carbon dioxide under acidic conditions. The COD of the liquid sample was determined using Colorimetric Determination Method 8000 to study the degree of mineralization after photocatalytic degradation. In this research, the vials containing samples mixed with digestion reagents were subjected to heating in the COD reactor for 2 hours. Subsequently, low range COD test was conducted.

CHAPTER 4

RESULTS AND DISCUSSIONS

4.1 Characterisation of Photocatalysts

4.1.1 XRD

The crystal phases of the pure TiO_2 , AC and AC/ TiO_2 composite at various compositions were analysed using the XRD. Figure 4.1 shows the XRD patterns. The pattern for AC showed broad peaks indicating that the sample was poorly crystallized. The broad diffraction peak at $2\theta = 21.4^\circ$ matched the reflexions in the (002) plane of amorphous carbon matrix (Omri, et al., 2014). The other two diffraction peaks at $2\theta = 64.3^\circ$ and 77.5° were contributed by other minerals such as SiO_2 -cristoballite and SiO_2 -quartz particles which were found to be very common in AC (Quiñones, et al., 2014).

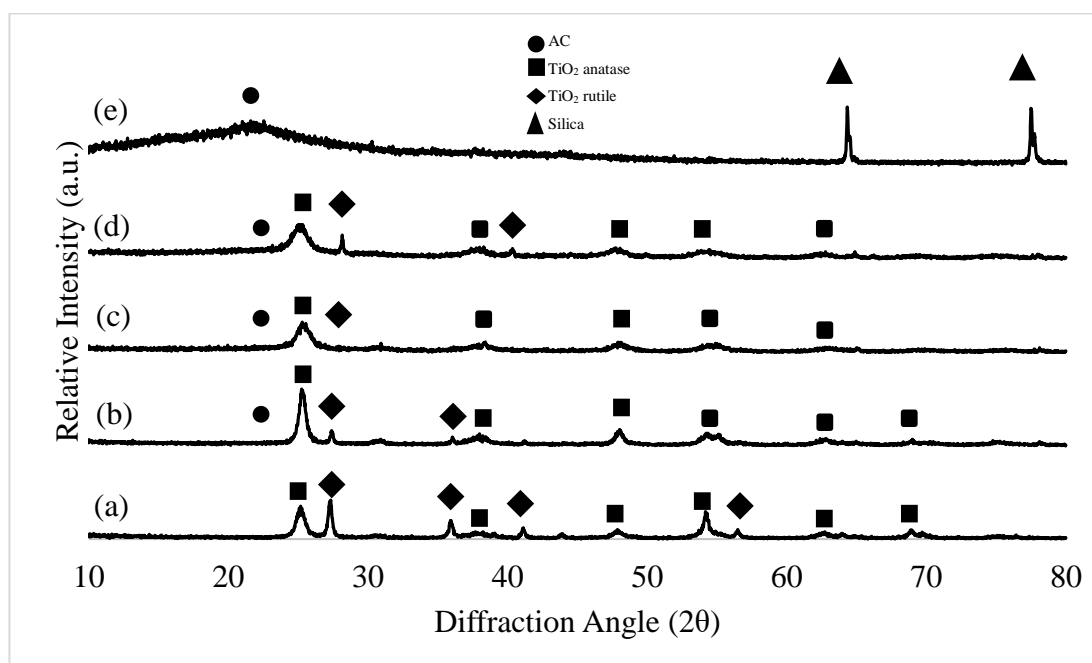


Figure 4.1: XRD Patterns for (a) Pure TiO_2 , AC/ TiO_2 Composite at Weight Ratio (b) 1:3, (c) 1:1, (d) 3:1 and (e) Pure AC

For pure TiO_2 , the XRD patterns showed some characteristic peaks. The diffraction peaks at $2\theta = 25.2^\circ$, 37.7° , 47.8° , 54.2° , 62.6° and 68.9° referred to the

(101), (004), (200), (105), (204) and (115) crystal planes of the TiO₂ anatase phase, respectively (Muniandy, et al., 2016; Meng, et al., 2014). Peaks at $2\theta = 27.3^\circ$, 35.9° , 41.1° and 56.4° corresponded to the (110), (101), (111) and (220) crystal planes of TiO₂ rutile phase (Larsen, et al., 2011). It was observed that there were more peaks corresponding to the anatase phase than the rutile phase. The small amount of rutile phase could have been formed during the calcination process as the transformation from anatase to rutile phase occurs around 600-1100 °C (M. Baek, et al., 2013).

As for the AC/TiO₂ composite at various compositions, the diffraction peaks were similar to those found in the XRD patterns of pure AC and TiO₂ anatase phase. However, it can be observed that the number of peaks corresponding to TiO₂ rutile phase had decreased. It was also observed that increasing the amount of AC in the AC/TiO₂ composites reduced the average peak intensity of the rutile phase. Hence, this proved that combining AC and TiO₂ together helped in limiting the transformation of anatase to rutile phase. This led to better photocatalytic properties because anatase is normally more active and efficient as compared to rutile phase (Omri, et al., 2014). In addition, broader peaks were observed on all the AC/TiO₂ composites which might be due to the combined effect from peaks corresponding to the AC samples.

The average crystallite size of the various samples was calculated using the Debye-Scherrer equation (Equation 2.9). The average sizes of various samples are represented in Table 4.1. It was observed that the crystallite sizes decreased with increasing amount of AC in the AC/TiO₂ composite. This might led to larger surface area for TiO₂ to be attached to the AC which in turn promotes the adsorption followed by oxidation ability of the composite samples (Sharma and Lee, 2017).

Table 4.1: Average Crystallite Sizes for Pure TiO₂, AC and AC/TiO₂ at Various Weight Ratio

Sample	Average Crystallite Size (nm)
TiO ₂	51.99
AC/TiO ₂ = 1:3	9.54
AC/TiO ₂ = 1:1	7.20
AC/TiO ₂ = 3:1	6.60
AC	80.18

Generally, the average crystallite sizes were very small which could be due to the high water to titanium precursor ratio used for the preparation of the TiO₂ particles. As a result, hydrolysis occurred much faster than condensation. The growth of the particles was inhibited by the rapid rate of nucleation and hence produced very fine sizes of the particles (Asiltürk and Sener, 2012).

4.1.2 SEM-EDX

The surface morphology of the pure AC, TiO₂ and AC/TiO₂ composite at various compositions was studied using SEM as depicted in Figure 4.2. As seen in Figure 4.2(a), the shape of the TiO₂ particles was mainly spherical and clustered together (Muthirulan, et al., 2013). On the other hand, the morphology of the AC was mainly smooth tubular structure with some pores that were developed because of the activation with KOH as seen in Figure 4.2(e) (Sivakumar Natarajan, et al., 2016). The average diameter of the pure TiO₂ was in the range of 1-50 nm which was very close to the estimation of mean crystallite size obtained from the XRD analysis.

Based on Figure 4.2(b) to (d), the amount of TiO₂ particles decreased while the AC loading was increased. Generally, the morphology of all three AC/TiO₂ composites showed that TiO₂ particles were attached successfully on the AC surface. The tubular structure of the AC can still be seen with a higher degree of porosity as compared to pure AC. Most of the TiO₂ particles were agglomerated and remained on the AC surface instead of entering the pores. Rajendran, et al. (2014) also reported that there was agglomeration of TiO₂ particles on AC after it was subjected to calcination at elevated temperature. This was attributed to the shrinking of TiO₂ precursors occurring during heat treatment (Shi, et al., 2012). The AC/TiO₂ composite at weight ratio 3:1 showed the well distribution of TiO₂ and limited particles agglomeration. As such, it did not limit the amount of organic pollutants to be adsorbed into the pores and hence allowed more TiO₂ particles to undergo photoexcitation process.

Besides, Muthirulan, et al. (2013) and Singh, et al. (2016) had captured similar images of TiO₂ particles being immobilized on the carbon surface. They found that agglomerations of TiO₂ mainly occurred on the surface rather than inside the pores which indicated that more TiO₂ particles were exposed to light and being photo-excited to produce the hydroxyl radicals (Zeng, et al., 2013). This could account for the significant increase in the photodegradation efficiency.

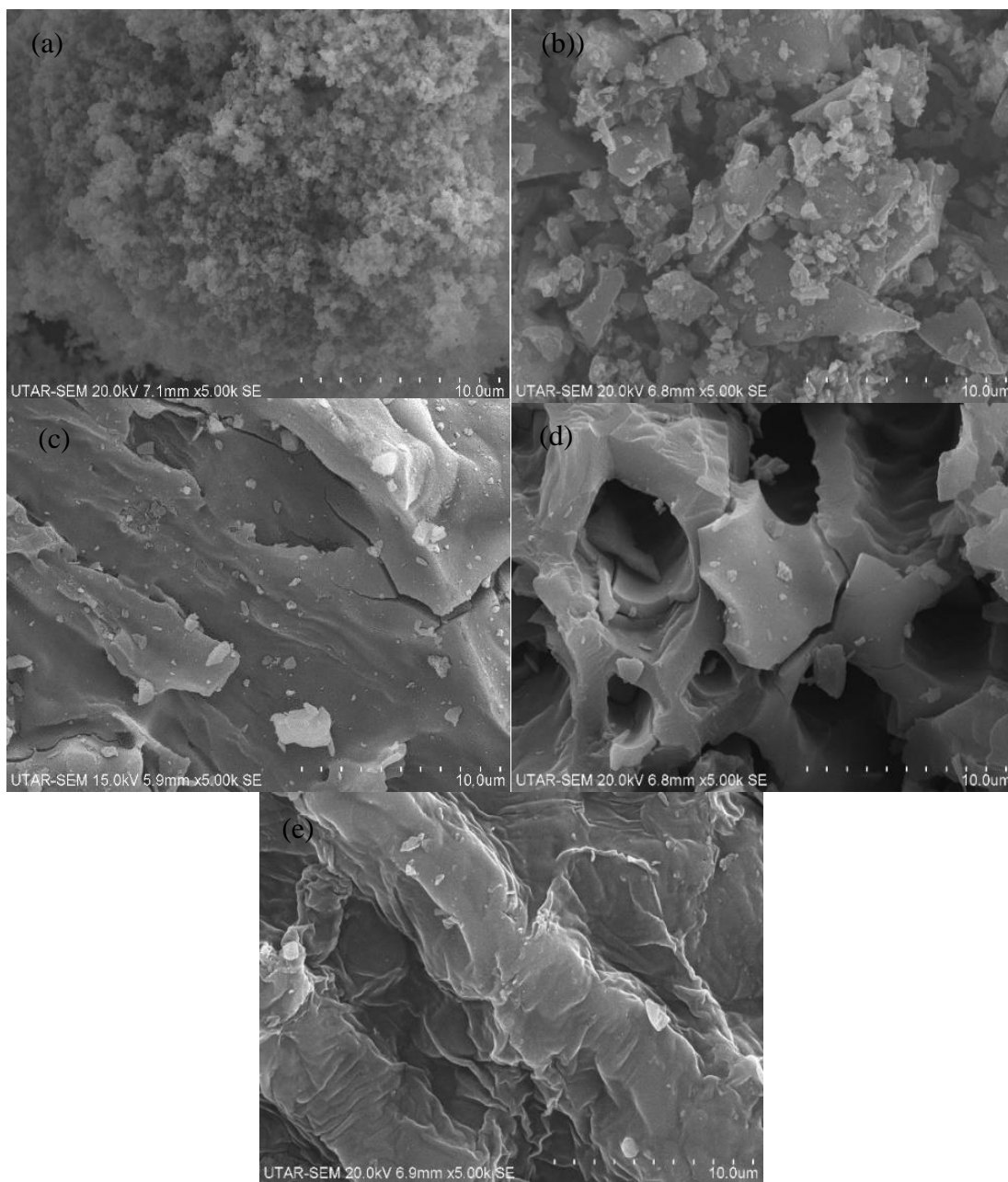


Figure 4.2: SEM Images of (a) Pure TiO_2 , AC/ TiO_2 Composite at Weight Ratio (b) 1:3, (c) 1:1, (d) 3:1 and (e) Pure AC

Table 4.2 summarizes the distribution of elements in the various samples. The result shows that TiO_2 consists of only Ti and O elements while only C, O and K elements were present in pure AC sample.

Table 4.2: Distribution of Elements in Various Samples

Sample	C (wt.%)	O (wt.%)	Ti (wt.%)	Si (wt.%)	Cl (wt.%)	K (wt.%)
TiO ₂	-	1.35	98.65	-	-	-
AC/TiO ₂ = 1:3	29.42	21.46	44.29	-	1.95	2.88
AC/TiO ₂ = 1:1	40.11	16.58	14.82	25.75	1.51	1.23
AC/TiO ₂ = 3:1	67.24	5.32	13.90	-	6.35	7.20
AC	80.44	10.60	-	-	-	8.96

The EDX analysis of AC/TiO₂ at various compositions have C, O and Ti as the majority elements and some other impurity elements such as Si, Cl and K. The presence of the inorganic elements had also been reported by Sharma and Lee (2017) and Orha, et al. (2017) who had found the presence of impurities such as Cl, P and Al in their samples. The presence of K and Cl elements could be due to chemicals such as KOH used for activation and Cl atoms in water, respectively. El-Sheikh, et al. (2017) and Singh, et al. (2016) had also reported similar type of elements present in their EDX analysis. The weight percentage of carbon element increased as the carbon proportion in AC/TiO₂ composite samples increases. Thus, it can be said that the TiO₂ particles had been properly incorporated on the AC surface with good dispersity.

4.1.3 FT-IR Spectroscopy

The active surface functional groups on the pure AC, TiO₂ and AC/TiO₂ composite at various compositions was studied using FT-IR Spectroscopy as shown in Figure 4.3. All five spectra showed a broad band at about 3400 cm⁻¹, 2380 cm⁻¹ and a sharper peak at 1600 cm⁻¹ which were corresponded to the stretching mode of hydroxyl (O-H) vibration in water (Singh, et al., 2016; Gar Alalm, et al., 2016). During the sol-gel preparation process, there was a possibility for TiO₂-OH bands formation during hydrolysis and this was confirmed by the observed peak (Ragupathy, et al., 2015). The stretching vibration could also be due to the presence of alcohol. The presence of Ti-OH was believed to prevent the recombination of holes and electrons during photocatalysis so that the photo-generated holes produce more reactive hydroxyl radicals (Nasirian, et al., 2017).

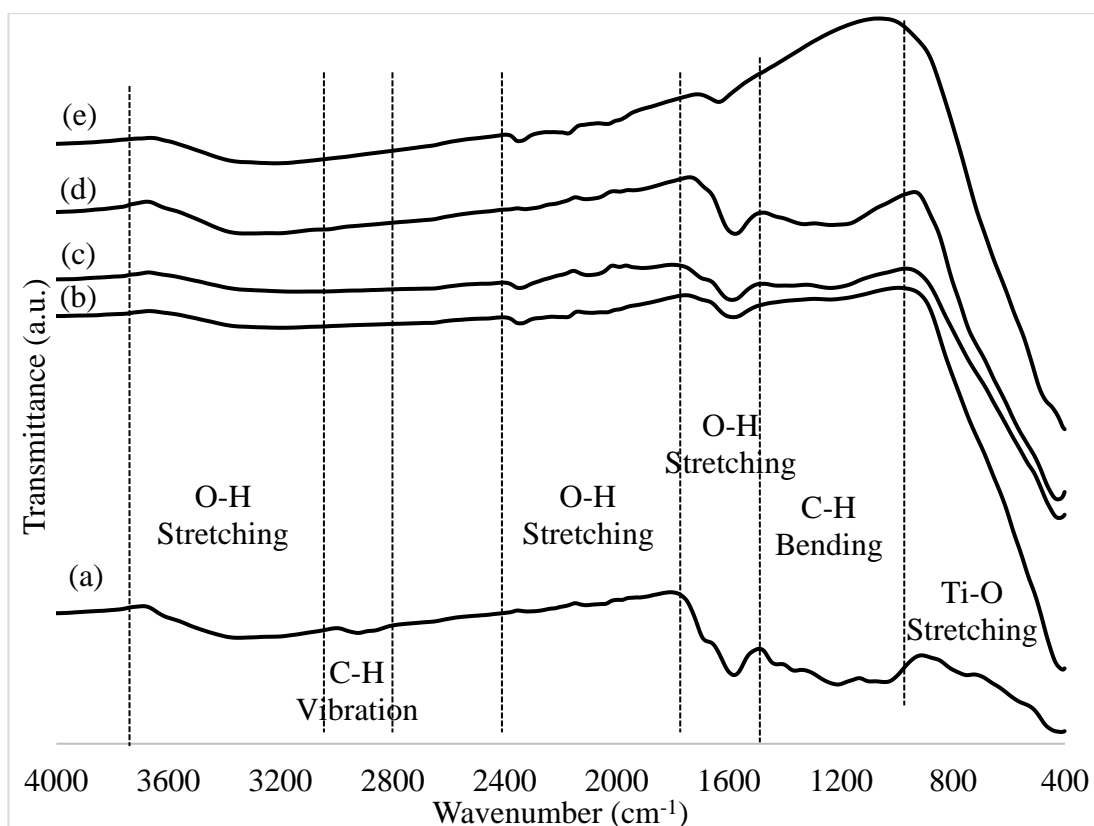


Figure 4.3: FT-IR Spectra for (a) Pure AC, AC/TiO₂ Composite at Weight Ratio (b) 1:3, (c) 1:1, (d) 3:1 and (e) Pure AC

On the other hand, the broad band at 400 cm⁻¹ to 960 cm⁻¹ corresponded to the stretching vibration of Ti-O which was caused by the presence of TiO₂ (Belayachi, et al., 2015). C-H stretching vibration of the alkane group was also observed as indicated by the broad peak at 2960 cm⁻¹. This could have originated from the titanium precursor and isopropanol used in the catalyst preparation (Ragupathy, et al., 2015). The peak at 1200 cm⁻¹ referred to the C-H bending modes (Meng, et al., 2014). It was observed that the width of the peak corresponding to C-H bending became narrower as a result of increased amount of AC in the composite. The peak width for Ti-O stretching decreased with the reduction in the amount of TiO₂ particles added. The results obtained from this FT-IR analysis was in good agreement with those obtained from the EDX analysis.

4.1.4 TGA

The thermal stability of the pure AC, TiO₂ and AC/TiO₂ composite at weight ratio 3:1 was determined through TGA as depicted in Figure 4.4. The TGA curves showed

that the AC/TiO₂ and pure AC samples first exhibited weight loss of about 4.95 % and 5.81 %, respectively between 30 to 95 °C. This was due to the evaporation of water molecules embedded in the pores and surface of the catalysts (Muniandy, et al., 2016).

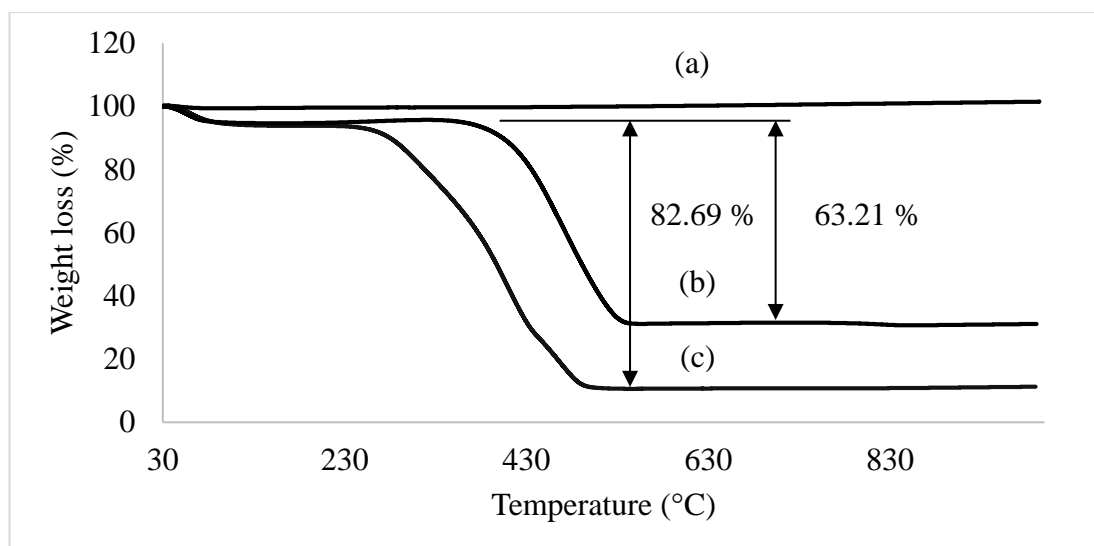


Figure 4.4: TGA Curves for (a) Pure TiO₂, (b) AC/TiO₂ Composite at Weight Ratio 1:3 and (c) Pure AC

The second weight loss occurred from 200 to 550 °C and was observed to be about 63.21 % for AC/TiO₂. As for pure AC, the weight loss happened between 200 to 500 °C and was calculated to be 82.69 %. This was due to the decomposition of carbon. It was observed that the weight loss was much lower for the composite sample as compared to the pure AC suggesting that the doping of TiO₂ particles on AC had increased the thermal stability of the catalyst. In addition, the amount of carbon lost (63.21 %) in AC/TiO₂ sample was also in close agreement with the carbon amount recorded in the EDX study. Meanwhile, pure TiO₂ experienced negligible weight loss (0.733 %) around 30 °C which was due to the loss of water and insignificant weight loss between temperatures 200-900 °C. Similar result was also obtained by Dinari and Haghghi (2017) suggesting that pure TiO₂ had extremely high thermal stability.

4.1.5 BET Analysis

The specific surface area of the AC/TiO₂ composite was determined from the nitrogen adsorption-desorption isotherm at 77 K and calculated using the BET method. From the analysis, the specific surface area of the AC/TiO₂ composite at weight ratio 3:1 was found to be 150.49 m²/g. This is about 3 times higher than commercial P25 TiO₂ (Degussa Co., Germany) that has a specific surface area of 50 m²/g (Reza, et al., 2015). This was an indication that TiO₂ particles were successfully incorporated into the AC. The AC acted as a doping agent for TiO₂ (Martins, et al., 2017). Studies conducted by Omri, et al. (2014) and M. H. Baek, et al. (2013) recorded similar increment in specific surface area of AC/TiO₂ composite as compared to TiO₂.

From literature, commercial AC has specific surface area between 500 to 1500 m²/g (Hidayu and Muda, 2016). The specific surface area of AC/TiO₂ composite obtained from the BET analysis was much lower than pure AC because there was blockage of the AC pores and deposition on external surface by TiO₂ particles (Sivakumar Natarajan, et al., 2016). Similar observations were recorded by Asiltürk and Sener (2012). It was argued that the calcination process had induced the formation of anatase TiO₂ on the surface and pores of the AC (Gar Alalm, et al., 2016).

In short, AC/TiO₂ of weight ratio 3:1 had relatively higher surface area than TiO₂. The increased surface area allowed more TiO₂ particles to be embedded on the surface and pores of the AC. The increased surface adsorption could have allowed more hydroxyl radicals to be formed and further enhanced the degradation efficiency of the dye molecules.

4.2 Parameter Studies

4.2.1 Effect of Various Types of Organic Dyes

The effect of photocatalytic degradation of various dyes using AC/TiO₂ composite was studied. The result is shown in Figure 4.5. Five organic dyes were used, namely, Congo Red, Methylene Blue, Rhodamine B, Reactive Blue 4 and Malachite Green. It was observed that the photocatalytic degradation efficiency of Malachite Green was the highest, then followed by Methylene Blue, Rhodamine B, Congo Red and lastly Reactive Blue 4.

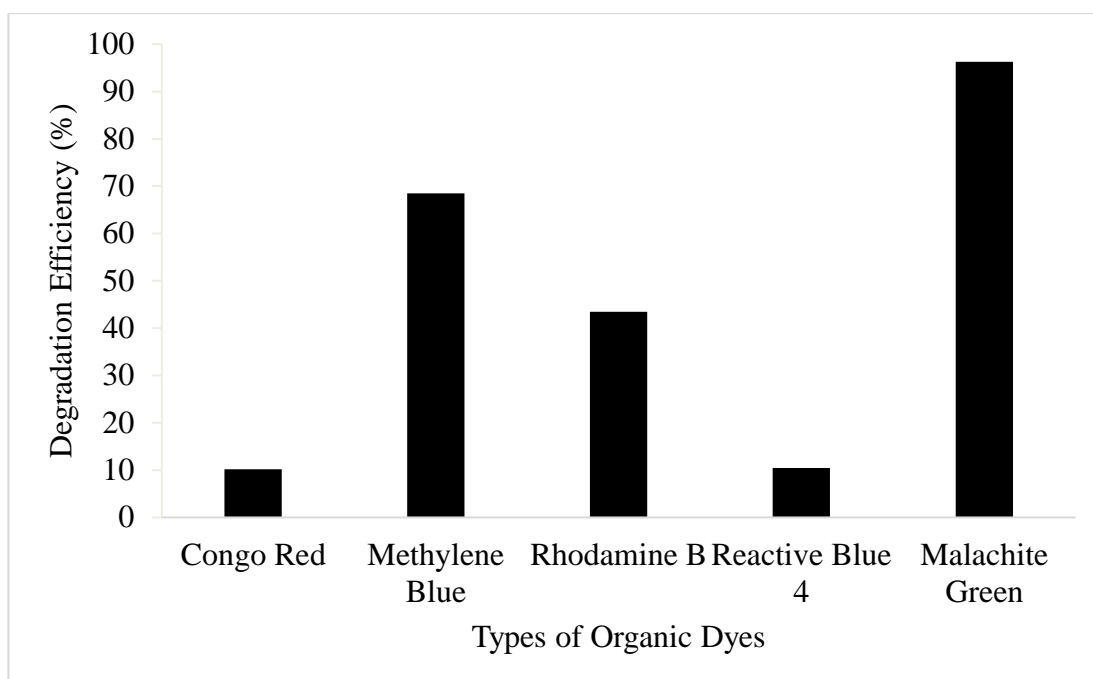


Figure 4.5: Photocatalytic Degradation of Various Organic Dyes by AC/TiO₂ Composite at Weight Ratio 3:1 (Catalyst Loading = 2.5 g/L, Initial Dye Concentration = 10 mg/L, Solution Temperature = 50 °C, Reaction Time = 7.5 minutes)

Šíma and Hasal (2013) claimed that the differences in degradation efficiency could be attributed to the different dye molecular weights. It is harder for dye molecules with high molecular weight to enter the small pores of the support layer. This subsequently reduced the adsorption of dye molecules on the surface of TiO₂ particles which are important for photodegradation (Šíma and Hasal, 2013). The molecular weights of Malachite Green and Methylene Blue are similar (364.911 g/mol and 319.85 g/mol, respectively). Their molecular weights are significantly lower than the 3 other dyes. This accounted for the significantly higher degradation efficiency as compared with the rest of the dyes. The molecular weights of Rhodamine B, Congo Red and Reactive Blue 4 are 479.01 g/mol, 696.66 g/mol and 637.419 g/mol, respectively. Congo Red and Reactive Blue 4 recorded the least degradation efficiency as expected because they have the highest molecular weight.

Besides that, the degradation efficiency was affected by the chemical structures of the dye molecules (Rao and Venkatarangiah, 2014). Malachite Green is a basic triphenylmethane and dicationic dye that was reported to have the best degradation efficiency in the presence of strong oxidising agents and hydroxyl

radicals (Muhd Julkapli, et al., 2014). Methylene Blue and Rhodamine B are also basic cationic dye and thus had similar degradation efficiency as Malachite Green (Liu, et al., 2015). On the other hand, Congo Red is an azo dye which contains azo bond (-N=N-) with aromatic rings. It was claimed that this type of dye was very stable and cannot be easily degraded under light (Muhd Julkapli, et al., 2014). Lastly, the lowest degradation efficiency recorded with Reactive Blue 4 could be due to the presence of sulfo ($-\text{SO}_3^-$) electron-withdrawing groups (Khataee, et al., 2015).

4.2.2 Adsorption and Photocatalytic Performance of AC/TiO₂ Composites

The adsorption capacity and effect of different AC/TiO₂ composite at various weight ratio (0:1, 1:3, 1:1, 3:1 and 1:0) on the photocatalytic degradation of Malachite Green was studied. The result is illustrated in Figure 4.6 and 4.7 respectively. The adsorption capacity generally increased with the percentage of AC in the AC/TiO₂ composite. Meanwhile, the photocatalytic degradation efficiency of the dye also increased with the percentage of AC in the AC/TiO₂ composite. The degradation

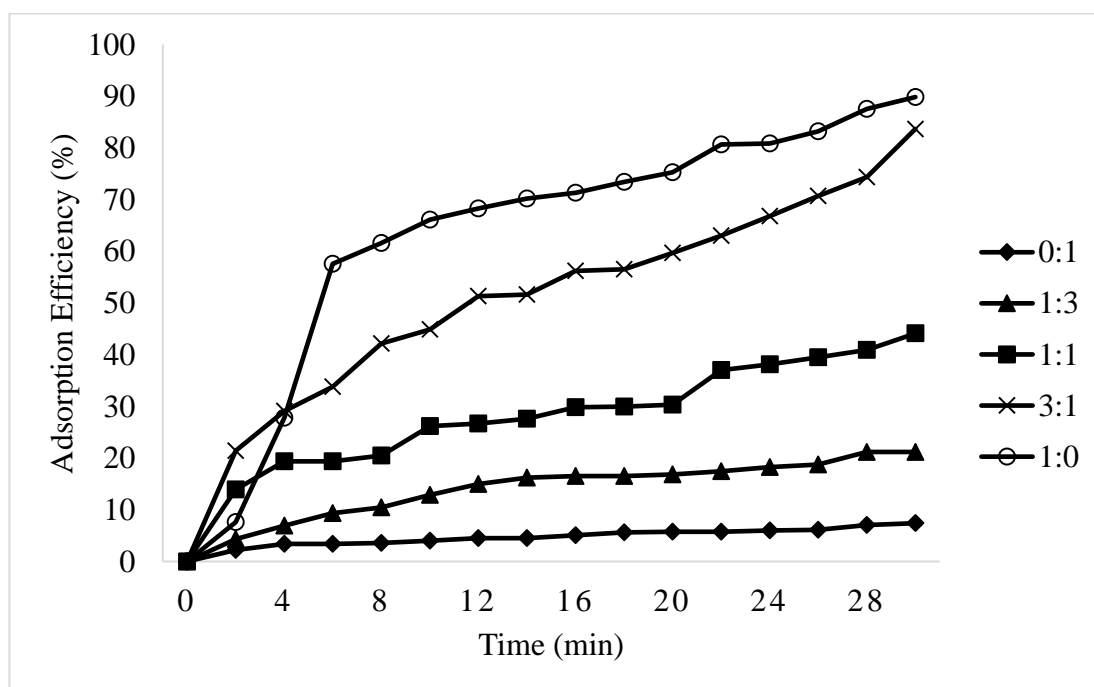


Figure 4.6: Adsorption Capacity of Malachite Green by Pure AC, TiO₂ and AC/TiO₂ Composite at Various Weight Ratio (Catalyst Loading = 2.5 g/L, Initial Dye Concentration = 10 mg/L, Solution Temperature = 30 °C, Reaction Time = 30 minutes)

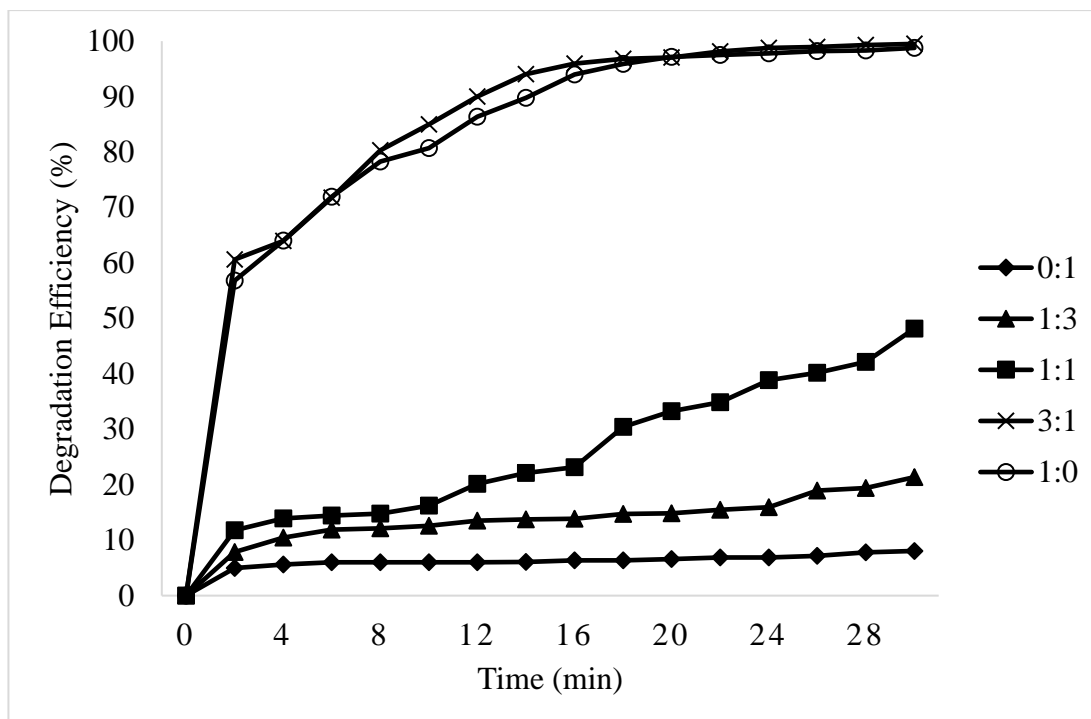


Figure 4.7: Photocatalytic Degradation of Malachite Green by Pure AC, TiO₂ and AC TiO₂ Composite at Various Weight Ratio (Catalyst Loading = 2.5 g/L, Initial Dye Concentration = 10 mg/L, Solution Temperature = 30 °C, Reaction Time = 30 minutes)

efficiency using AC/TiO₂ composite at weight ratio 0:1, 1:3 and 1:1 recorded moderate degradation efficiency at 8.06 %, 21.4 % and 48.2 %, respectively. However, the degradation efficiency improved significantly to 99.5 % when 3:1 AC/TiO₂ was used.

There were several reasons for the increased degradation efficiency when more AC was used. Firstly, the incorporation of AC into the TiO₂ microstructure prevented the recombination of photogenerated electron-hole pairs. This was also due to the more effective injection of excited electron onto the surface of the carbon which then promotes the photocatalysis process (Cheng, et al., 2016). Besides that, the addition of AC into TiO₂ reduced the band gap energy needed for electron excitation and hence range of the excitation wavelength became larger. Not only that, AC itself has high surface area which effectively increased the surface area for the adsorption of reactant onto the catalyst surface. On top of that, the activated carbon could have made the TiO₂ microstructure more thermodynamically stable, inhibit the

growth of TiO₂ crystallites and helped in retaining the hydroxyl groups on the surface (Omri, et al., 2014).

Similar positive results have been recorded by Xing, et al. (2016) in the photocatalytic degradation of Rhodamine B. These results showed that there was a synergistic effect between AC and TiO₂. The adsorption capacity of AC/TiO₂ composite at weight ratio 1:0 was much higher than AC/TiO₂ composite at weight ratio 3:1. This was an indication that the degradation of Malachite Green was mainly due to adsorption and not photocatalysis. The optimal composition of AC/TiO₂ was at weight ratio 3:1 because it exhibited the highest degradation efficiency that can be attributed to both adsorption and photocatalysis process.

4.2.3 Effect of Catalyst Loading

The effect of catalyst loading (0.5, 1.0, 1.5, 2.0 and 2.5 g/L) was investigated on the photocatalytic degradation of Malachite Green. The result is shown in Figure 4.8. It was noted that the lowest degradation efficiency was recorded using 0.5 g/L composite. Upon increasing the loading from 1.0 g/L up to 2.5 g/L, there was a significant improvement in the degradation of Malachite Green, whereby the efficiency increased up to 99.5 % in 30 minutes. The increment of degradation efficiency started to decrease when the catalyst loading was increased from 1.5 g/L to 2.5 g/L.

The significant increment in degradation efficiency could be attributed to the increase in available sites for dye adsorption and number of photons adsorbed that in turn produced more free radicals that degrade the dye molecules (Ragupathy, et al., 2015). Meanwhile, at higher catalyst loading, the screening effect became prominent. There was a reduction in the amount of light penetration into the dye solution despite the increase in available adsorption sites (Muthirulan, et al., 2013). When there was not enough energy to overcome the band gap energy of the AC/TiO₂ composite, no free radicals were produced and hence decreased photocatalytic activity.

Previous works conducted by Xing, et al. (2016) and Ng, et al. (2016) on the photocatalytic degradation of Rhodamine B and Malachite Green, respectively confirmed the increment observations. Therefore, the amount of catalyst used highly influenced the rate of degradation. The optimal loading of catalyst was determined to be 2.5 g/L because it exhibited the highest degradation efficiency.

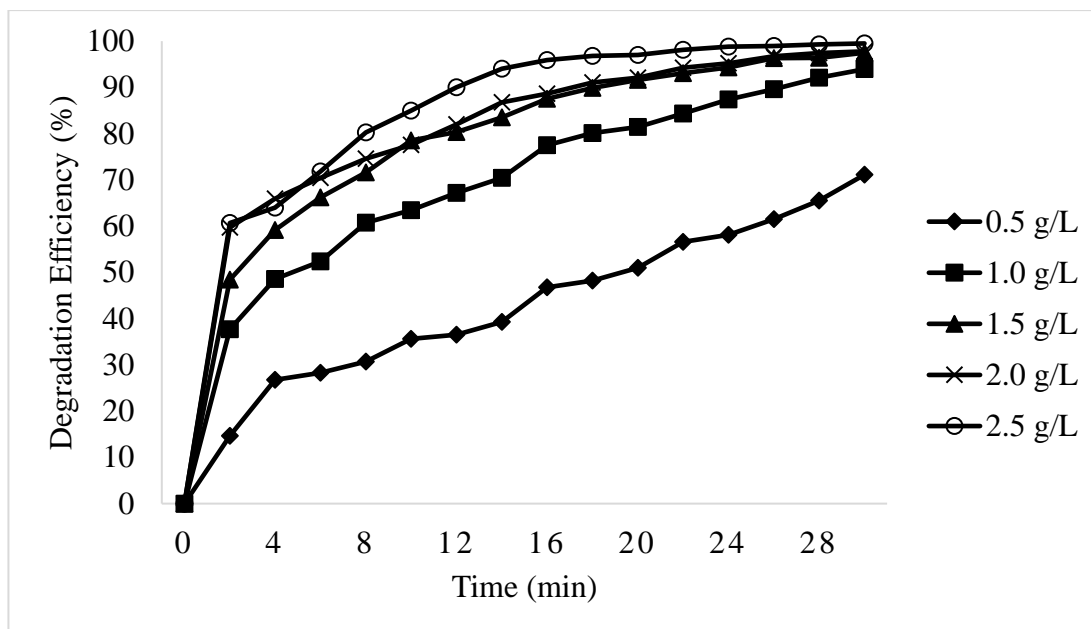


Figure 4.8: Effect of Catalyst Loading on the Photocatalytic Degradation of Malachite Green in the Presence of AC/TiO₂ Catalyst at Weight Ratio 3:1 (Initial Dye Concentration = 10 mg/L, Solution Temperature = 30 °C, Reaction Time = 30 minutes)

4.2.4 Effect of Initial Dye Concentration

The effect of initial dye concentration (10, 20, 30, 40 and 50 mg/L) was studied on the photocatalytic degradation of Malachite Green. The result is portrayed in Figure 4.9. From observation, the degradation efficiency decreased from 99.5 % to 32.5 % when the concentration of the dye was increased from 10 mg/L to 50 mg/L.

The decrease in degradation efficiency was attributed to the reduced path length of photons into the dye solution. As a result, most of the light energy was absorbed by the dye instead of the catalyst itself (Sobana, et al., 2013). At the same time, the adsorption sites on the catalyst quickly became saturated because of the increase in initial dye concentration (Yagub, et al., 2014). Thus, the decrement in degradation efficiency was due to the insufficient catalytic sites for the dye molecules to adsorb and react with hydroxyl radicals (Zangeneh, et al., 2015).

In short, the higher the initial concentration of Malachite Green, the lower is the degradation efficiency. The highest degradation efficiency was achieved with the initial concentration of Malachite Green at 10 mg/L.

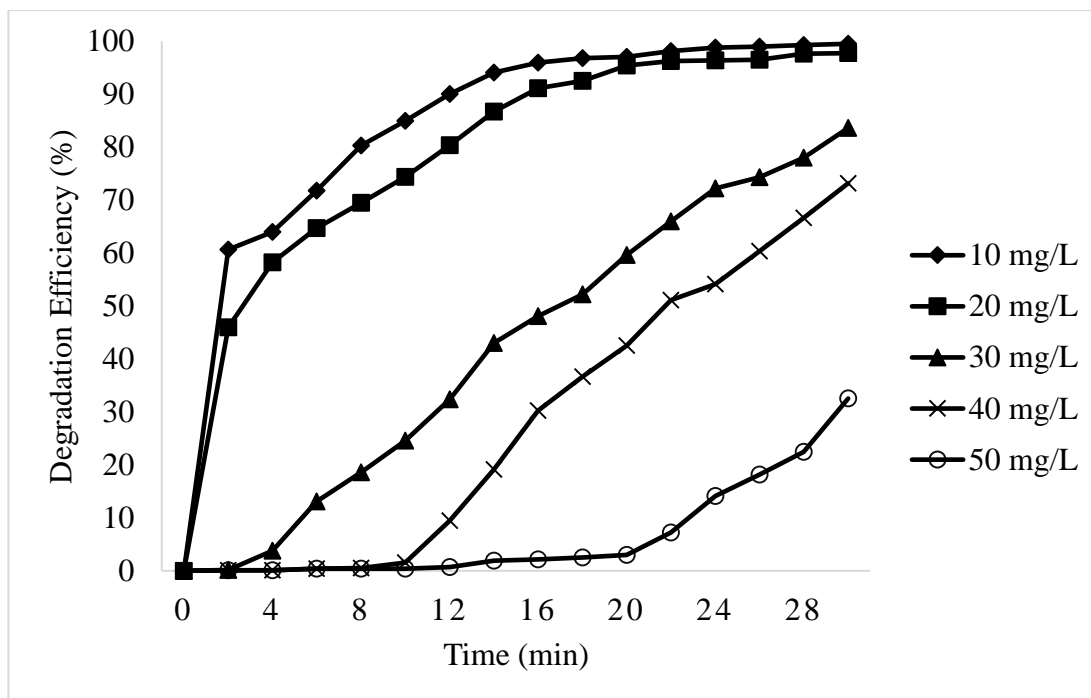


Figure 4.9: Effect of Initial Dye Concentration on the Photocatalytic Degradation of Malachite Green in the Presence of AC/TiO₂ Catalyst at Weight Ratio 3:1 (Catalyst Loading = 2.5 g/L, Solution Temperature = 30 °C, Reaction Time = 30 minutes)

4.2.5 Effect of Solution Temperature

The effect of solution temperature (30, 40, 50, 60 and 70 °C) on the photocatalytic degradation of Malachite Green was investigated. The result is represented in Figure 4.10. It was found that the degradation efficiency was strongly influenced by the solution temperature. The degradation efficiency increased from 84.0 % to 99.4 % when the solution temperature was increased from 30 °C to 70 °C. However, the degradation efficiency differences between 50 °C and 70 °C was minimal. At these higher solution temperatures, the time required for the dye molecules to be degraded was shorter. In 30 seconds, the degradation efficiency of Malachite Green was 56.2 % to 70.6 % at solution temperature of 50 °C to 70 °C while the degradation efficiency at 30 °C to 40 °C was only between 33.5 % to 48.6 %.

Since the degradation efficiency increased with increasing solution temperature, the photocatalytic degradation of Malachite Green was an endothermic process. The increased in degradation efficiency was due to the increased mobility of dye molecules at higher solution temperature. Thereby, increase in the number of active sites for adsorption and oxidation reaction (Yagub, et al., 2014). It was reported that electron-hole recombination occurred less frequently and hence the

oxidation rate of dye molecules by holes at the catalyst surface was increased (Zangeneh, et al., 2015).

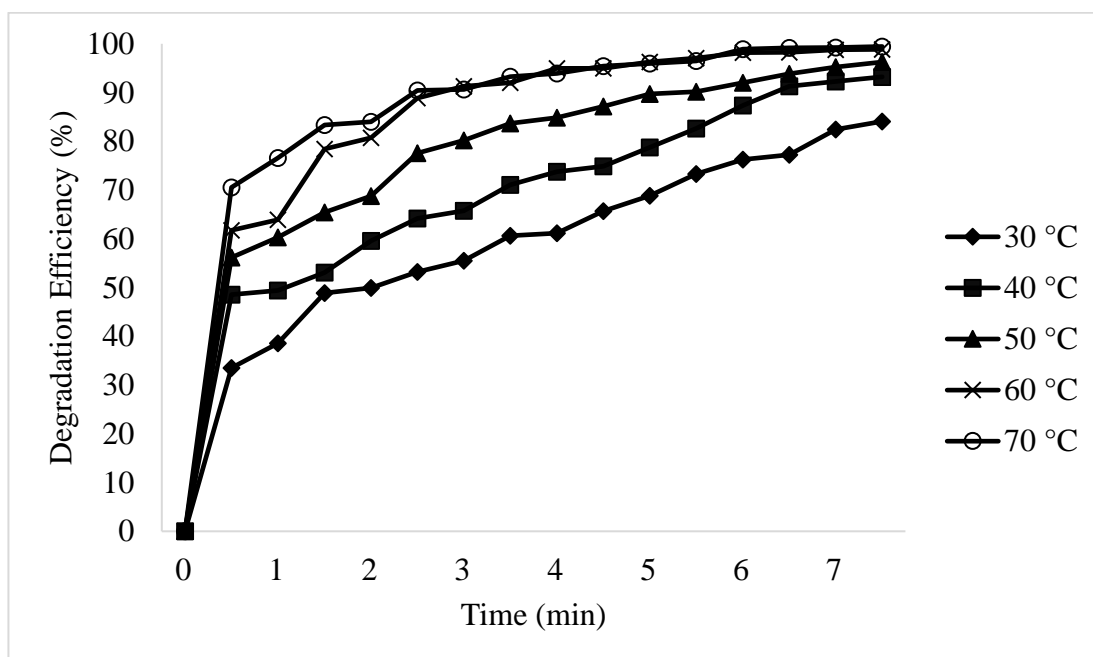


Figure 4.10: Effect of Solution Temperature on the Photocatalytic Degradation of Malachite in the Presence of AC/TiO₂ Catalyst at Weight Ratio 3:1 (Catalyst Loading = 2.5 g/L, Initial Dye Concentration = 10 mg/L, Reaction Time = 7.5 minutes)

Previous works conducted by Alhaji, et al. (2016) and Barka, et al. (2010) were in agreement with the above mentioned observations. In short, the photocatalytic degradation efficiency of Malachite Green can be improved by increasing solution temperature. The optimal temperature was taken as 50 °C although the degradation efficiency at 60 °C and 70 °C were higher, the differences were not that significant.

4.3 Reusability Study

The degradation efficiency of Malachite Green by the spent AC/TiO₂ composite at weight ratio 3:1 was studied. The spent catalyst was retrieved by thorough washing using distilled water for three times. Based on the Figure 4.11, the degradation efficiency of fresh AC/TiO₂ and reused AC/TiO₂ were 96.3 % and 83.1 %, respectively after 30 minutes. Hence, this indicated that the spent AC/TiO₂ can still

be used to degrade the dye molecules but there was minimal performance reduction of the catalyst in photocatalytic efficiency.

There were a few researchers who reported similar decrement results. Wang, et al. (2016) reported that AC-based magnetic TiO_2 co-doped with Iodine and Nitrogen experienced decrement in photocatalytic degradation efficiency from 89.71 % to 75.78 % after five runs. Besides that, Kamalakkannan, et al. (2015) also claimed that the AC loaded TiO_2 co-doped with Nitrogen and Sulphur showed a decrease in photodegradation of Malachite Green from 100 % to 95 % after five runs. Hence, there was strong evidence that the AC/ TiO_2 composite can be reused and showed potential in its usage in wastewater treatment as a cheap and reliable alternative.

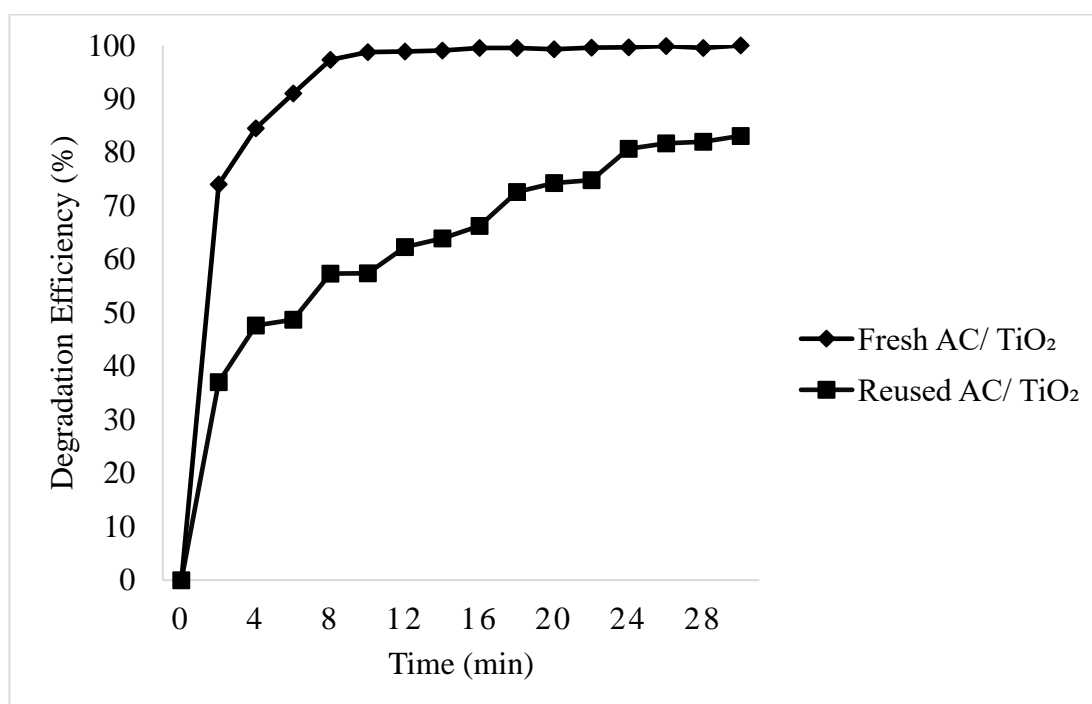


Figure 4.11: Photocatalytic Degradation of Malachite Green by Fresh and Reused AC/ TiO_2 Catalyst at Weight Ratio 3:1 (Catalyst Loading = 2.5 g/L, Initial Dye Concentration = 10 mg/L, Solution Temperature = 50 °C, Reaction Time = 30 minutes)

4.4 Kinetic Study

Kinetic studies were conducted on the photocatalytic degradation of Malachite Green in order to find out the reaction order of the process. The pseudo zero, first and second-order kinetic expressions were studied on the experimental data obtained using 10 mg/L Malachite Green at different solution temperatures.

Figure 4.12 shows a plot of $\ln(C_0/C_t)$ against time (t) for five different solution temperatures. In all cases, linear lines were drawn to regress the data points. The photocatalytic degradation efficiency can be said to follow a pseudo first-order kinetic because of the relatively high R^2 value as compared to that of pseudo zero and second-order kinetics. This was in agreement to the results obtained by other researchers such as Sobana, et al. (2013) who studied the photocatalytic degradation of Direct Yellow 4 and Chen, et al. (2016) who investigated on the photocatalytic degradation of cefradine. They both concluded that photocatalytic degradation followed the pseudo first-order kinetic model. The gradients of the linear lines are the apparent first-order rate constants (k_{app}). The values of R^2 and k_{app} are shown in Table 4.3. Generally, the rate constant increased tremendously from 0.2415 to 0.6221 min^{-1} as the solution temperature was increased from 30 °C to 70 °C. This was caused by the increase in collision frequency of molecules that resulted in the generation of more hydroxyl radicals (Choquette-Labbé, et al., 2014).

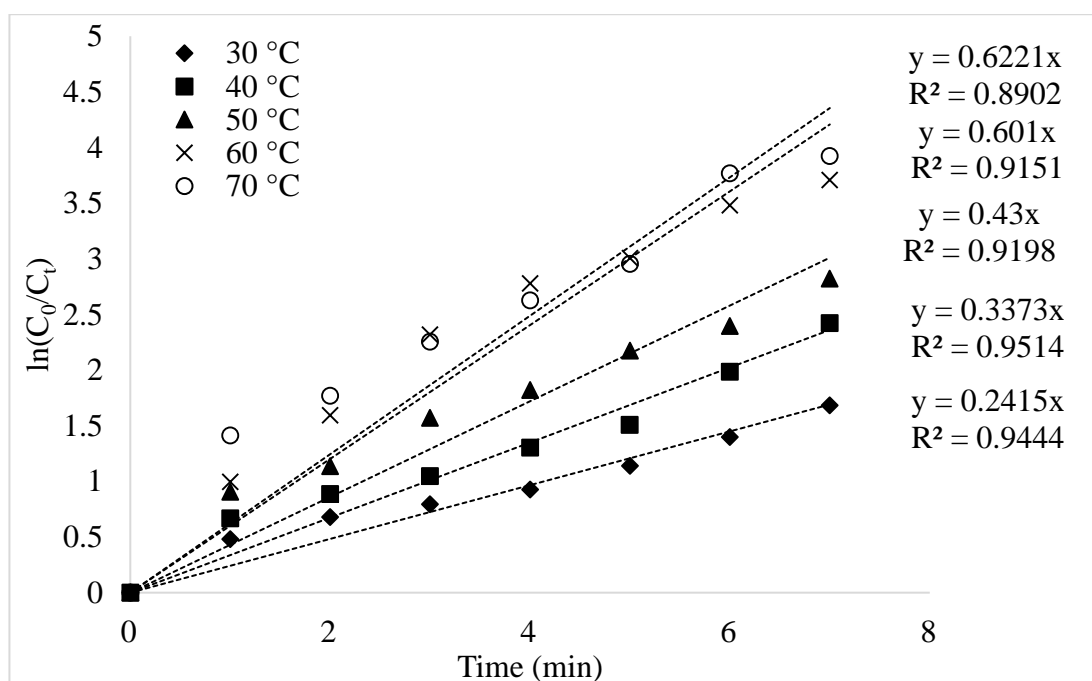


Figure 4.12: Pseudo First-Order Reaction Kinetics Plot for Photocatalytic Degradation of Malachite Green

Table 4.3: Reaction Rate Constants for Photocatalytic Degradation of Malachite Green by AC/TiO₂ Composite at Weight Ratio 3:1 under Different Solution Temperatures

Temperature (°C)	Pseudo zero-order model		Pseudo first-order model		Pseudo second-order model	
	R^2	k_{app}	R^2	k_{app}	R^2	k_{app}
		$\frac{\text{mg}}{\text{L}\cdot\text{min}}$		$\frac{1}{\text{min}}$		$\frac{\text{L}}{\text{mg}\cdot\text{min}}$
30	0.6648	1.4225	0.9444	0.2415	0.9128	0.0492
40	0.5404	1.6080	0.9514	0.3373	0.7990	0.1027
50	0.2838	1.7763	0.9198	0.4300	0.8903	0.1717
60	0.1424	1.8575	0.9151	0.6010	0.8948	0.4737
70	0	1.9429	0.8902	0.6221	0.7991	0.5397

The relationship between k_{app} and solution temperature can be explained using the Arrhenius equation as shown previously in Equation 2.12. By plotting $\ln k_{app}$ against $1/T$ for the five different solution temperatures, all the parameters in the equation can be obtained. According to Figure 4.13, a satisfactory relationship between $\ln k_{app}$ and $1/T$ was obtained because of the high R^2 value of 0.9676. The complete Arrhenius equation for the photocatalytic degradation of Malachite Green is shown in Equation 4.1.

$$\ln k_{app} = 7.1435 - 2583.6 \left(\frac{1}{T} \right) \quad (4.1)$$

The value of E_a was determined by finding the gradient ($-E_a/R$). With R being a constant, E_a can be calculated easily. The value of A was obtained from the intercept. The values of E_a and A for the photocatalytic degradation of Malachite Green under different temperatures were 21.48 kJ/mol and $1.27 \times 10^3 \text{ min}^{-1}$, respectively. The E_a value was lower than the recorded value (65.4 kJ/mol) by Yetim and Tekin (2017) in the photocatalytic degradation of textile dyes. It was also lower than the E_a value (32.95 kJ/mol) obtained by Barka et al. (2010) for the photocatalytic degradation of Reactive Yellow 84 which meant that the photodegradation of Malachite Green occurred more readily and easily.

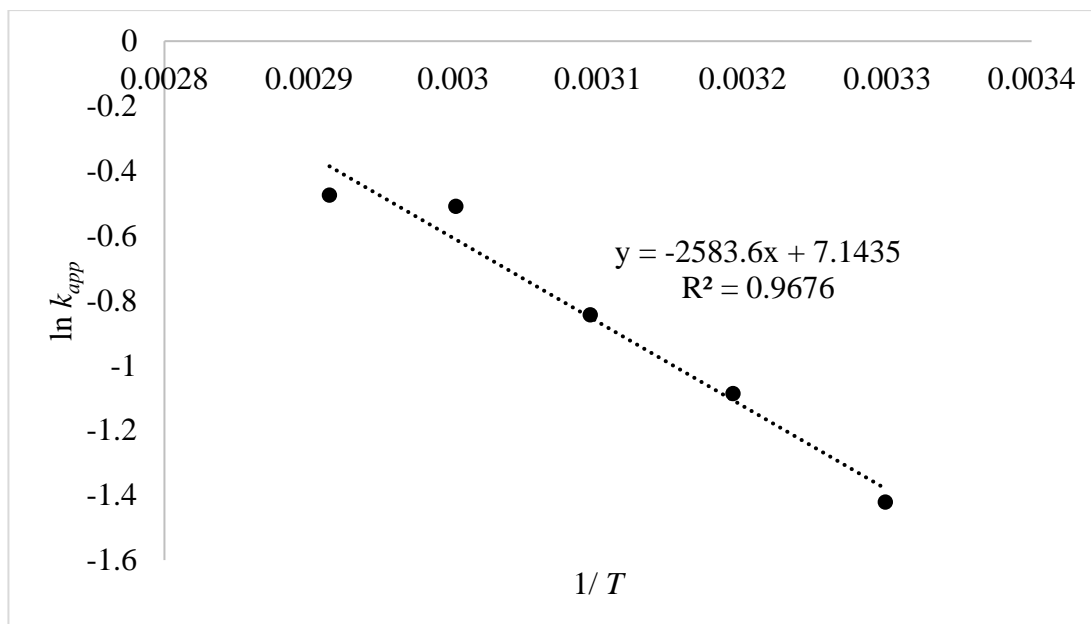


Figure 4.13: Arrhenius Plot of $\ln k_{app}$ against $1/T$

4.5 Liquid Sample Analysis

4.5.1 COD Results

The COD removal by the photocatalytic degradation process of Malachite Green was studied. The COD values of the liquid sample with the optimum condition (AC/TiO₂ catalyst = 3:1, catalyst loading = 2.5 g/L, initial dye concentration = 10 mg/L, solution temperature = 50 °C, reaction time = 30 minutes) for the instance before and after the photocatalytic reaction had been determined by Colorimetric Determination Method 8000.

It was observed that after 30 minutes, 96.7 % of the COD had been removed from the liquid sample. This COD result was in close agreement with the dye degradation efficiency results obtained in the parameter studies. Similar findings had been reported by other researchers. Asiltürk and Sener (2012) reported COD reduction as high as 93 % after 110 minutes using AC/TiO₂ for the photocatalytic degradation of Rhodamine B. On the other hand, Belayachi, et al. (2015) observed significantly high removal of COD (98 %) from Reactive Black 5 after 1 hour of photocatalytic degradation using UV light. Therefore, it can be inferred that the addition of AC into TiO₂ had produced an enhanced adsorption effect, light absorption ability and reduced electron-hole recombination which significantly

improved the Malachite Green dye removal performance (Sivakumar Natarajan, et al., 2016).

CHAPTER 5

CONCLUSIONS AND RECOMMENDATIONS

5.1 Conclusions

In this research, a novel AC/TiO₂ composite was synthesized using sol-gel method for the purpose of photocatalytic degradation of Malachite Green. The characteristics of the AC/TiO₂ composite were investigated using XRD, SEM-EDX, FT-IR, TGA and BET analysis. The XRD patterns suggested that anatase and rutile phase TiO₂ particles were successfully embedded on the AC surface in the sample. The SEM results indicated that the AC/TiO₂ composite was made up of spherical TiO₂ particles agglomerated on the smooth tubular and porous structure of AC. The EDX analysis demonstrated that the AC/TiO₂ composite was mainly composed of Ti, O and C atoms. FT-IR spectroscopy indicated the presence of O-H stretching, C-H vibration and bending as well as Ti-O stretching in the AC/TiO₂ composites. The specific surface area of the AC/TiO₂ composite at weight ratio 3:1 obtained through BET analysis was found to be 150.49 m²/g which was much higher than P25 TiO₂. It was noted that the AC/TiO₂ composite had significantly better performance in the photocatalytic degradation of Malachite Green as compared to pure AC and TiO₂ individually.

The effect of various parameters such as various types of organic dyes, weight proportion of AC/TiO₂, catalyst loading, initial dye concentration and solution temperature were studied on the photocatalytic degradation of Malachite to find out the optimum conditions. It was discovered that increasing the amount of AC in AC/TiO₂ enhanced the photocatalytic efficiency. The degradation of Malachite Green was attributed to the adsorption and photocatalysis processes. The optimum conditions for the degradation process were determined to be 2.5 g/L of AC/TiO₂ at weight ratio 3:1 used on an initial dye concentration of 10 mg/L at 50 °C. In these conditions, the degradation efficiency was 96.3 % in 7.5 minutes. Almost complete removal of COD (96.7 %) was also recorded.

Besides, the reusability of AC/TiO₂ composite in the photodegradation of dye was also investigated. The recycled composite recorded only minor decrease in catalytic activity and managed to achieve a degradation efficiency of 83.1 % for the

second catalytic cycle. Kinetic studies on the photocatalytic degradation of Malachite Green were also performed. The photocatalytic degradation process was observed to follow pseudo first-order kinetics. The values of E_a and A for the degradation of Malachite Green were 21.48 kJ/mol and $1.27 \times 10^3 \text{ min}^{-1}$, respectively.

5.2 Recommendations for future work

The specific surface area of AC/TiO₂ at different weight ratio should also be determined using BET surface analysis in order to study the effect of different weight proportion on the porosity and specific surface area. The specific surface area is an important property of catalyst as it affects photocatalytic degradation efficiency. Larger surface area might indicate more TiO₂ particles can be embedded onto the surface and pores of the AC. This can then lead to more TiO₂ particles being excited and producing more hydroxyl radicals that will increase the degradation of dye molecules. Thus, it is important to determine the highest specific surface area among various AC/TiO₂ composite at different weight ratio.

On top of that, Inductively Coupled Plasma- Optical Emission Spectroscopy (ICP-OES) can also be employed in the characterisation of the AC/TiO₂ composite. ICP-OES is an efficient analytical tool that can be used to discover trace Ti element. By using this technique, the impurities that were found in the synthesis of AC/TiO₂ composite can be traced and tracked back to its origins so that precautionary steps can be taken in the future to avoid contamination.

REFERENCES

- Adhikari, S. and Sarkar, D., 2015. Metal oxide semiconductors for dye degradation. *Materials Research Bulletin*, 72, pp. 220–228.
- Ahmed, S., Rasul, M.G., Martens, W.N., Brown, R. and Hashib, M.A., 2010. Heterogeneous photocatalytic degradation of phenols in wastewater: A review on current status and developments. *Desalination*, 261(1–2), pp. 3–18.
- Akpan, U.G. and Hameed, B.H., 2009. Parameters affecting the photocatalytic degradation of dyes using TiO₂-based photocatalysts: A review. *Journal of Hazardous Materials*, 170(2–3), pp. 520–529.
- Alhaji, M.H., Sanaullah, K., Lim, S.F., Khan, A., Hipolito, C.N., Abdullah, M.O., Bhawani, S.A. and Jamil, T., 2016. Photocatalytic treatment technology for palm oil mill effluent (POME) - A review. *Process Safety and Environmental Protection*, 102, pp. 673–686.
- Altin, I., Sokmen, M. and Biyiklioglu, Z., 2016. Sol gel synthesis of cobalt doped TiO₂ and its dye sensitization for efficient pollutant removal. *Materials Science in Semiconductor Processing*, 45, pp. 36–44.
- Asenjo, N.G., Santamaría, R., Blanco, C., Granda, M., Álvarez, P. and Menéndez, R., 2013. Correct use of the Langmuir-Hinshelwood equation for proving the absence of a synergy effect in the photocatalytic degradation of phenol on a suspended mixture of titania and activated carbon. *Carbon*, 55, pp. 62–69.
- Asiltürk, M. and Sener, S., 2012. TiO₂-activated carbon photocatalysts : Preparation, characterization and photocatalytic activities. *Chemical Engineering Journal*, 180, pp. 354–363.
- Baek, M., Jung, W., Yoon, J., Hong, J., Lee, Y. and Suh, J., 2013. Preparation, characterization and photocatalytic activity evaluation of micro- and mesoporous TiO₂/spherical activated carbon. *Journal of Industrial and Engineering Chemistry*, 19(2), pp. 469–477.
- Baek, M.H., Yoon, J.W., Hong, J.S. and Suh, J.K., 2013. Application of TiO₂-containing mesoporous spherical activated carbon in a fluidized bed photoreactor-Adsorption and photocatalytic activity. *Applied Catalysis A: General*, 450, pp. 222–229.
- Barka, N., Qourzal, S., Assabbane, A., Nounah, A. and Ait-Ichou, Y., 2010. Photocatalytic degradation of an azo reactive dye, Reactive Yellow 84, in water using an industrial titanium dioxide coated media. *Arabian Journal of Chemistry*, 3(4), pp. 279–283.

Bazrafshan, E., Alipour, M.R. and Mahvi, A.H., 2015. Textile wastewater treatment by application of combined chemical coagulation , electrocoagulation , and adsorption processes. *Desalination and Water Treatment*, 57, pp. 9203–9215.

Belayachi, H., Bestani, B., Benderdouche, N. and Belhakem, M., 2015. The use of TiO₂ immobilized into grape marc-based activated carbon for RB-5 Azo dye photocatalytic degradation. *Arabian Journal of Chemistry*. [online] Available at: <<http://dx.doi.org/10.1016/j.arabjc.2015.06.040>> [Accessed 26 July 2017].

Bilinska, L., Gmurek, M. and Ledakowicz, S., 2016. Comparison between industrial and simulated textile wastewater treatment by AOPs- Biodegradability, toxicity and cost assessment. *Chemical Engineering Journal*, 306, pp. 550–559.

Chen, J., Shu, J., Anqi, Z., Juyuan, H., Yan, Z. and Chen, J., 2016. Synthesis of carbon quantum dots/TiO₂ nanocomposite for photo-degradation of Rhodamine B and cefradine. *Diamond and Related Materials*, 70, pp. 137–144.

Chen, M.L., Lim, C.S. and Oh, W.C., 2007. Preparation with different mixing ratios of anatase to activated carbon and their photocatalytic performance. *Journal of Ceramic Processing Research*, 8(2), pp. 119–124.

Cheng, C.K., Deraman, M.R., Ng, K.H. and Khan, M.R., 2016. Preparation of titania doped argemone photocatalyst and its photoactivity towards palm oil mill effluent degradation. *Journal of Cleaner Production*, 112, pp. 1128–1135.

Cheng, G., Xu, F., Xiong, J., Tian, F., Ding, J., Stadler, F.J. and Chen, R., 2016. Enhanced adsorption and photocatalysis capability of generally synthesized TiO₂-carbon materials hybrids. *Advanced Powder Technology*, 27(5), pp. 1949–1962.

Choquette-Labbé, M., Shewa, W., Lalman, J. and Shanmugam, S., 2014. Photocatalytic degradation of phenol and phenol derivatives using a nano-TiO₂ catalyst: Integrating quantitative and qualitative factors using response surface methodology. *Water*, 6(6), pp. 1785–1806.

Choudhury, A.K.R., 2006. *Textile Preparation and Dyeing*. New Hampshire: Science Publishers.

Clark, M., 2011. Fundamental principles of dyeing. In: *Handbook of Textile and Industrial Dyeing*. Amsterdam: Elsevier, pp. 3–27.

Danks, A.E., Hall, S.R. and Schnepf, Z., 2016. The evolution of “sol–gel” chemistry as a technique for materials synthesis. *Materials Horizons*, 3, pp. 91–112.

Department of Environment Malaysia, 2010. *Environment Quality (Industrial Effluents) Regulations 2009*, DOE Malaysia, Malaysia.

Department of Environment Malaysia, 2015. *Malaysia Environmental Quality Report 2015*, Kuala Lumpur.

Diak, M., Grabowska, E. and Zaleska, A., 2015. Synthesis, characterization and photocatalytic activity of noble metal-modified TiO₂ nanosheets with exposed {0 0 1} facets. *Applied Surface Science*, 347, pp. 275–285.

Dinari, M. and Haghghi, A., 2017. Surface modification of TiO₂ nanoparticle by three dimensional silane coupling agent and preparation of polyamide/modified-TiO₂ nanocomposites for removal of Cr(VI) from aqueous solutions. *Progress in Organic Coatings*, 110(April), pp. 24–34.

Dulov, A., Dulova, N. and Trapido, M., 2011. Combined physicochemical treatment of textile and mixed industrial wastewater. *Ozone: Science and Engineering*, 33(4), pp. 285–293.

El-Sheikh, S.M., Khedr, T.M., Hakki, A., Ismail, A.A., Badawy, W.A. and Bahnemann, D.W., 2017. Visible light activated carbon and nitrogen co-doped mesoporous TiO₂ as efficient photocatalyst for degradation of ibuprofen. *Separation and Purification Technology*, 173, pp. 258–268.

Foo, K.Y. and Hameed, B.H., 2010. Decontamination of textile wastewater via TiO₂/activated carbon composite materials. *Advances in Colloid and Interface Science*, 159(2), pp. 130–143.

Gao, N., Lu, Z., Zhao, X., Zhu, Z., Wang, Y., Wang, D., Hua, Z., Li, C., Huo, P. and Song, M., 2016. Enhanced photocatalytic activity of a double conductive C/Fe₃O₄/Bi₂O₃ composite photocatalyst based on biomass. *Chemical Engineering Journal*, 304, pp. 351–361.

Gar Alalm, M., Tawfik, A. and Ookawara, S., 2016. Enhancement of photocatalytic activity of TiO₂ by immobilization on activated carbon for degradation of pharmaceuticals. *Journal of Environmental Chemical Engineering*, 4(2), pp. 1929–1937.

Georgiou, D., Melidis, P., Aivasidis, A. and Gimouhopoulos, K., 2002. Degradation of azo-reactive dyes by ultraviolet radiation in the presence of hydrogen peroxide. *Dyes and Pigments*, 52(2), pp. 69–78.

Gomathi Devi, L. and Mohan Reddy, K., 2010. Enhanced photocatalytic activity of silver metallized TiO₂ particles in the degradation of an azo dye methyl orange: Characterization and activity at different pH values. *Applied Surface Science*, 256(10), pp. 3116–3121.

Günay, M., 2013. *Eco-friendly Textile Dyeing and Finishing*. Rijeka: InTech.

Gupta, V.K. and Suhas, 2009. Application of low-cost adsorbents for dye removal - A review. *Journal of Environmental Management*, 90(8), pp. 2313–2342.

Gürses, A., Açıkyıldız, M., Güneş, K. and Gürses, M.S., 2016. *Dyes and Pigments*. Cham: Springer International Publishing.

Hameed, B.H., Tan, I.A.W. and Ahmad, A.L., 2009. Preparation of oil palm empty fruit bunch-based activated carbon for removal of 2,4,6-trichlorophenol: Optimization using response surface methodology. *Journal of Hazardous Materials*, 164(2–3), pp. 1316–1324.

Hidayu, A.R. and Muda, N., 2016. Preparation and characterization of impregnated activated carbon from palm kernel shell and coconut shell for CO₂ capture. *Procedia Engineering*, 148, pp. 106–113.

Hunger, K., 2003. *Industrial dyes: chemistry, properties, applications*. 3rd ed. Weinheim: Wiley-VCH.

IBP Inc., 2016. *India chemicals and petrochemicals industry business opportunities handbook - Strategic information and contacts*. Washington: Lulu.com.

Ibrahim, I., Hassan, M.A., Abd-Aziz, S., Shirai, Y., Andou, Y., Othman, M.R., Ali, A.A.M. and Zakaria, M.R., 2017. Reduction of residual pollutants from biologically treated palm oil mill effluent final discharge by steam activated bioadsorbent from oil palm biomass. *Journal of Cleaner Production*, 141, pp. 122–127.

Kalliala, E. and Talvenmaa, P., 2000. Environmental profile of textile wet processing in Finland. *Journal of Cleaner Production*, 8(2), pp. 143–154.

Kamalakkannan, J., Chandraboss, V.L., Prabha, S. and Senthilvelan, S., 2015. Activated carbon loaded N, S co-doped TiO₂ nanomaterial and its dye wastewater treatment. *International Letters of Chemistry, Physics and Astronomy*, 47, pp. 147–164.

Khataee, A., Vahid, B., Akbarpour, A. and Aber, S., 2015. Effect of dye chemical structure on the efficiency of photoassisted electrochemical degradation using a cathode containing carbon nanotubes and a Ti/RuO₂ anode. *Research on Chemical Intermediates*, 41(9), pp. 6073–6085.

Konstantinou, I.K. and Albanis, T.A., 2004. TiO₂-assisted photocatalytic degradation of azo dyes in aqueous solution: Kinetic and mechanistic investigations: A review. *Applied Catalysis B: Environmental*, 49(1), pp. 1–14.

Larsen, G.K., Fitzmorris, R., Zhang, J.Z. and Zhao, Y., 2011. Structural, optical, and photocatalytic properties of Cr:TiO₂ nanorod array fabricated by oblique angle codeposition. *The Journal of Physical Chemistry C*, 115, pp. 16892–16903.

Lau, W.J. and Ismail, A.F., 2009. Polymeric nanofiltration membranes for textile dye wastewater treatment: Preparation, performance evaluation, transport modelling, and fouling control - a review. *Desalination*, 245(1–3), pp. 321–348.

Leary, R. and Westwood, A., 2011. Carbonaceous nanomaterials for the enhancement of TiO₂ photocatalysis. *Carbon*, 49(3), pp. 741–772.

Li Puma, G., Bono, A. and Collin, J.G., 2008. Preparation of titanium dioxide photocatalyst loaded onto activated carbon support using chemical vapor deposition: A review paper. *Journal of Hazardous Materials*, 157(2–3), pp. 209–219.

Liu, L., Zhang, B., Zhang, Y., He, Y., Huang, L., Tan, S. and Cai, X., 2015. Simultaneous removal of cationic and anionic dyes from environmental water using montmorillonite-pillared graphene oxide. *Journal of Chemical and Engineering Data*, 60(5), pp. 1270–1278.

Liu, T., Wang, L., Lu, X., Fan, J., Cai, X., Gao, B., Miao, R., Wang, J. and Lv, Y., 2017. Comparative study of the photocatalytic performance for the degradation of different dyes by ZnIn₂S₄: adsorption, active species, and pathways. *RSC Adv.*, 7(20), pp. 12292–12300.

Liu, W.-W., Chai, S.-P., Mohamed, A.R. and Hashim, U., 2014. Synthesis and characterization of graphene and carbon nanotubes: A review on the past and recent developments. *Journal of Industrial and Engineering Chemistry*, 20(4), pp. 1171–1185.

Liu, X., Chen, G. and Su, C., 2011. Effects of material properties on sedimentation and aggregation of titanium dioxide nanoparticles of anatase and rutile in the aqueous phase. *Journal of Colloid and Interface Science*, 363(1), pp. 84–91.

Liu, Z., Andreev, Y.G., Robert Armstrong, A., Brutti, S., Ren, Y. and Bruce, P.G., 2013. Nanostructured TiO₂(B): the effect of size and shape on anode properties for Li-ion batteries. *Progress in Natural Science: Materials International*, 23(3), pp. 235–244.

Luttrell, T., Halpegamage, S., Tao, J., Kramer, A., Sutter, E. and Batzill, M., 2014. Why is anatase a better photocatalyst than rutile? - Model studies on epitaxial TiO₂ films. *Scientific Reports*, 4(4043), pp. 1–8.

Ma, C., Wang, F., Zhang, C., Yu, Z., Wei, J., Yang, Z., Li, Y., Li, Z., Zhu, M., Shen, L. and Zeng, G., 2017. Photocatalytic decomposition of Congo red under visible light irradiation using MgZnCr-TiO₂ layered double hydroxide. *Chemosphere*, 168, pp. 80–90.

Mahmoodi, N.M., Arami, M. and Zhang, J., 2011. Preparation and photocatalytic activity of immobilized composite photocatalyst (titania nanoparticle/activated carbon). *Journal of Alloys and Compounds*, 509(14), pp. 4754–4764.

Mano, T., Nishimoto, S., Kameshima, Y. and Miyake, M., 2015. Water treatment efficacy of various metal oxide semiconductors for photocatalytic ozonation under UV and visible light irradiation. *Chemical Engineering Journal*, 264, pp. 221–229.

Marcucci, M., Ciabatti, I., Matteucci, A. and Vernaglione, G., 2003. Membrane technologies applied to textile wastewater treatment. *Annals of the New York Academy of Sciences*, 984, pp. 53–64.

Martins, A.C., Cazetta, A.L., Pezoti, O., Souza, J.R.B., Zhang, T., Pilau, E.J., Asefa, T. and Almeida, V.C., 2017. Sol-gel synthesis of new TiO₂/activated carbon photocatalyst and its application for degradation of tetracycline. *Ceramics International*, 43(5), pp. 4411–4418.

McCusker, L.B., Liebau, F. and Engelhardt, G., 2003. Nomenclature of structural and compositional characteristics of ordered microporous and mesoporous materials with inorganic hosts (IUPAC recommendations 2001). *Microporous and Mesoporous Materials*, 58, pp. 3–13.

Meng, H., Hou, W., Xu, X., Xu, J. and Zhang, X., 2014. TiO₂-loaded activated carbon fiber: Hydrothermal synthesis, adsorption properties and photo catalytic activity under visible light irradiation. *Particuology*, 14, pp. 38–43.

Mezohegyi, G., van der Zee, F.P., Font, J., Fortuny, A. and Fabregat, A., 2012. Towards advanced aqueous dye removal processes: A short review on the versatile role of activated carbon. *Journal of Environmental Management*, 102, pp. 148–164.

Mohammadzadeh, S., Olya, M.E., Arabi, A.M., Shariati, A. and Khosravi Nikou, M.R., 2015. Synthesis, characterization and application of ZnO-Ag as a nanophotocatalyst for organic compounds degradation, mechanism and economic study. *Journal of Environmental Sciences (China)*, 35, pp. 194–207.

Mokhtar, N.M., Lau, W.J., Ismail, A.F., Kartohardjono, S., Lai, S.O. and Teoh, H.C., 2016. The potential of direct contact membrane distillation for industrial textile wastewater treatment using PVDF-Cloisite 15A nanocomposite membrane. *Chemical Engineering Research and Design*, 111, pp. 284–293.

Morali, E.K., Uzal, N. and Yetis, U., 2016. Ozonation pre and post-treatment of denim textile mill effluents: Effect of cleaner production measures. *Journal of Cleaner Production*, 137, pp. 1–9.

Muhd Julkapli, N., Bagheri, S. and Bee Abd Hamid, S., 2014. Recent advances in heterogeneous photocatalytic decolorization of synthetic dyes. *Scientific World Journal*. [online] Available at: <<https://www.hindawi.com/journals/tswj/2014/692307/>> [Accessed 26 July 2017].

Muniandy, L., Adam, F., Mohamed, A.R., Ng, E.P. and Rahman, N.R.A., 2016. Carbon modified anatase TiO₂ for the rapid photo degradation of methylene blue: A comparative study. *Surfaces and Interfaces*, 5, pp. 19–29.

Muthirulan, P., Nirmala Devi, C. and Meenakshi Sundaram, M., 2013. Synchronous role of coupled adsorption and photocatalytic degradation on CAC-TiO₂ composite generating excellent mineralization of alizarin cyanine green dye in aqueous solution. *Arabian Journal of Chemistry*, 10, pp. S1477–S1483.

Namasivayam, C. and Sumithra, S., 2005. Removal of direct red 12B and methylene blue from water by adsorption onto Fe (III)/Cr (III) hydroxide, an industrial solid waste. *Journal of Environmental Management*, 74(3), pp. 207–215.

Nasirian, M., Bustillo-lecompte, C.F. and Mehrvar, M., 2017. Photocatalytic efficiency of Fe₂O₃/TiO₂ for the degradation of typical dyes in textile industries : Effects of calcination temperature and UV-assisted thermal synthesis. *Journal of Environmental Management*, 196, pp. 487–498.

Nethaji, S., Tamilarasan, G., Neehar, P. and Sivasamy, A., 2017. Visible light photocatalytic activities of BiOBr-activated carbon (derived from waste polyurethane) composites by hydrothermal process. *Journal of Environmental Chemical Engineering*. [online] Available at: <<http://www.sciencedirect.com/science/article/pii/S2213343717300891>> [Accessed 26 July 2017].

Ng, K.H., Cheng, Y.W., Khan, M.R. and Cheng, C.K., 2016. Optimization of photocatalytic degradation of palm oil mill effluent in UV/ZnO system based on response surface methodology. *Journal of Environmental Management*, 184, pp. 487–493.

Ng, K.H., Lee, C.H., Khan, M.R. and Cheng, C.K., 2016. Photocatalytic degradation of recalcitrant POME waste by using silver doped titania: Photokinetics and scavenging studies. *Chemical Engineering Journal*, 286, pp. 282–290.

Omri, A., Lambert, S.D., Geens, J., Bennour, F. and Benzina, M., 2014. Synthesis, surface characterization and photocatalytic activity of TiO₂ supported on almond shell activated carbon. *Journal of Materials Science & Technology*, 30(9), pp. 894–902.

Orha, C., Pode, R., Manea, F., Lazau, C. and Bandas, C., 2017. Titanium dioxide-modified activated carbon for advanced drinking water treatment. *Process Safety and Environmental Protection*, 108, pp. 26–33.

Palominos, R.A., Mondaca, M.A., Giraldo, A., Peñuela, G., Pérez-Moya, M. and Mansilla, H.D., 2009. Photocatalytic oxidation of the antibiotic tetracycline on TiO₂ and ZnO suspensions. *Catalysis Today*, 144(1–2), pp. 100–105.

Pang, Y.L. and Abdullah, A.Z., 2013. Current status of textile industry wastewater management and research progress in Malaysia: A review. *Clean - Soil, Air, Water*, 41(8), pp. 751–764.

Pawar, R.C. and Lee, C.S., 2015. *Heterogeneous photocatalysts based on organic/inorganic semiconductor*. Amsterdam: Elsevier.

Quan, X., Luo, D., Wu, J., Li, R., Cheng, W. and Ge, Shuping, 2017. Ozonation of acid red 18 wastewater using $O_3/Ca(OH)_2$ system in a micro bubble gas-liquid reactor. *Journal of Environmental Chemical Engineering*, 5(1), pp. 283–291.

Quiñones, D.H., Rey, A., Álvarez, P.M., Beltrán, F.J. and Plucinski, P.K., 2014. Enhanced activity and reusability of TiO_2 loaded magnetic activated carbon for solar photocatalytic ozonation. *Applied Catalysis B: Environmental*, 144(1), pp. 96–106.

Rafatullah, M., Sulaiman, O., Hashim, R. and Ahmad, A., 2010. Adsorption of methylene blue on low-cost adsorbents: A review. *Journal of Hazardous Materials*, 177(1–3), pp. 70–80.

Ragupathy, S., Raghu, K. and Prabu, P., 2015. Synthesis and characterization of TiO_2 loaded cashew nut shell activated carbon and photocatalytic activity on BG and MB dyes under sunlight radiation. *Spectrochimica Acta - Part A: Molecular and Biomolecular Spectroscopy*, 138, pp. 314–320.

Rajendran, K., Senthil Kumar, V. and Anitha Rani, K., 2014. Synthesis and characterization of immobilized activated carbon doped TiO_2 thin films. *Optik - International Journal for Light and Electron Optics*, 125(8), pp. 1993–1996.

Ramachandran, P., Sundharam, R., Palaniyappan, J. and Munusamy, A.P., 2013. Potential process implicated in bioremediation of textile effluents: A review. *Pelagia Research Library Advances in Applied Science Research*, 4(1), pp. 131–145.

Rao, A.N.S. and Venkatarangaiah, V.T., 2014. The effect of cathode materials on indirect electrochemical oxidation of Methyl Orange, Malachite Green and Methylene Blue. *Portugaliae Electrochimica Acta*, 32(3), pp. 213–231.

Reza, K.M., Kurny, A.S.W. and Gulshan, F., 2015. Parameters affecting the photocatalytic degradation of dyes using TiO_2 : a review. *Applied Water Science*. [online] Available at: <<http://dx.doi.org/10.1007/s13201-015-0367-y>> [Accessed 26 July 2017].

Robati, D., 2013. Pseudo-second-order kinetic equations for modeling adsorption systems for removal of lead ions using multi-walled carbon nanotube. *Journal of Nanostructure in Chemistry*, 3(1), pp. 55.

Robinson, T., McMullan, G., Marchant, R. and Nigam, P., 2001. Remediation of dyes in textile effluent: A critical review on current treatment technologies with a proposed alternative. *Bioresource Technology*, 77(3), pp. 247–255.

Rodriguez-Reinoso, F. and Silvestre-Albero, J., 2016. Activated carbon and adsorption. *Reference Module in Materials Science*. [online] Available at: <<http://www.sciencedirect.com/science/article/pii/B978012803581802289X>> [Accessed 26 July 2017].

Roessler, A. and Jin, X., 2003. State of the art technologies and new electrochemical methods for the reduction of vat dyes. *Dyes and Pigments*, 59(3), pp. 223–235.

Saini, J., Garg, V.K., Gupta, R.K. and Kataria, N., 2017. Removal of Orange G and Rhodamine B dyes from aqueous system using hydrothermally synthesized zinc oxide loaded activated carbon (ZnO-AC). *Journal of Environmental Chemical Engineering*, 5(1), pp. 884–892.

Saravanan, R., Karthikeyan, S., Gupta, V.K., Sekaran, G., Narayanan, V. and Stephen, A., 2013. Enhanced photocatalytic activity of ZnO/CuO nanocomposite for the degradation of textile dye on visible light illumination. *Materials Science and Engineering C*, 33(1), pp. 91–98.

Sharma, A. and Lee, B.K., 2017. Growth of TiO₂ nano-wall on activated carbon fibers for enhancing the photocatalytic oxidation of benzene in aqueous phase. *Catalysis Today*, 287, pp. 113–121.

Shi, J.W., Cui, H.J., Chen, J.W., Fu, M.L., Xu, B., Luo, H.Y. and Ye, Z.L., 2012. TiO₂/activated carbon fibers photocatalyst: Effects of coating procedures on the microstructure, adhesion property, and photocatalytic ability. *Journal of Colloid and Interface Science*, 388(1), pp. 201–208.

Šíma, J. and Hasal, P., 2013. Photocatalytic degradation of textile dyes in a TiO₂/UV system. *Journal of Chemical Engineering Transactions*, 32(1999), pp. 79–84.

Singh, P., Vishnu, M.C., Sharma, K.K., Borthakur, A., Srivastava, P., Pal, D.B., Tiwary, D. and Mishra, P.K., 2016. Photocatalytic degradation of Acid Red dye stuff in the presence of activated carbon-TiO₂ composite and its kinetic enumeration. *Journal of Water Process Engineering*, 12, pp. 20–31.

Sivakumar Natarajan, T., Bajaj, H.C. and Tayade, R.J., 2016. Palmyra tuber peel derived activated carbon and anatase TiO₂ nanotube based nanocomposites with enhanced photocatalytic performance in rhodamine 6G dye degradation. *Process Safety and Environmental Protection*, 104, pp. 346–357.

Sobana, N., Krishnakumar, B. and Swaminathan, M., 2013. Synergism and effect of operational parameters on solar photocatalytic degradation of an azo dye (Direct Yellow 4) using activated carbon-loaded zinc oxide. *Materials Science in Semiconductor Processing*, 16(3), pp. 1046–1051.

Suib, S., 2013. New and future developments in catalysis. Catalysis by nanoparticles. In: *New and future developments in catalysis: Catalysis by Nanoparticles*. Amsterdam: Elsevier, pp. 213–244.

Tomei, M.C., Mosca Angelucci, D. and Daugulis, A.J., 2016. Sequential anaerobic-aerobic decolourization of a real textile wastewater in a two-phase partitioning bioreactor. *Science of the Total Environment*, 573, pp. 585–593.

Tseng, T.K., Lin, Y.S., Chen, Y.J. and Chu, H., 2010. A review of photocatalysts prepared by sol-gel method for VOCs removal. *International Journal of Molecular Sciences*, 11(6), pp. 2336–2361.

Unnikrishnan, P. and Srinivas, D., 2016. Chapter 3 - Heterogeneous Catalysis. In: Joshi, S.S. and Ranade, V. V, (eds.) *Industrial catalytic processes for fine and specialty chemicals*. Amsterdam: Elsevier, pp. 41–111.

Verma, A.K., Dash, R.R. and Bhunia, P., 2012. A review on chemical coagulation/flocculation technologies for removal of colour from textile wastewaters. *Journal of Environmental Management*, 93(1), pp. 154–168.

Victor-Ortega, M.D., Ochando-Pulido, J.M. and Martinez-Ferez, A., 2017. Impacts of main parameters on the regeneration process efficiency of several ion exchange resins after final purification of olive mill effluent. *Separation and Purification Technology*, 173, pp. 1–8.

Wang, X., Song, J., Huang, J., Zhang, J., Wang, X., Ma, R.R., Wang, J. and Zhao, J., 2016. Activated carbon-based magnetic TiO₂ photocatalyst codoped with iodine and nitrogen for organic pollution degradation. *Applied Surface Science*, 390, pp. 190–201.

Xing, B., Shi, C., Zhang, C., Yi, G., Chen, L., Guo, H., Huang, G. and Cao, J., 2016. Preparation of TiO₂/activated carbon composites for photocatalytic degradation of RhB under UV light irradiation. *Journal of Nanomaterials*, 2016, pp. 1–10.

Yagub, M.T., Sen, T.K., Afroze, S. and Ang, H.M., 2014. Dye and its removal from aqueous solution by adsorption: A review. *Advances in Colloid and Interface Science*, 209, pp. 172–184.

Yeoh, B.G., Environment Biotechnology Research Group Malaysia and Kementerian Sains, Teknologi dan Alam Sekitar, 1993. *Waste management in Malaysia: Current status and prospects for bioremediation : a monograph*. Kuala Lumpur: Ministry of Science, Technology and the Environment.

Yetim, T. and Tekin, T., 2017. A kinetic study on photocatalytic and sonophotocatalytic degradation of textile dyes. *Periodica Polytechnica: Chemical Engineering*, 61(2), pp. 102–108.

Yun, E.T., Yoo, H.Y., Kim, W., Kim, H.E., Kang, G., Lee, H., Lee, S., Park, T., Lee, C., Kim, J.H. and Lee, J., 2017. Visible-light-induced activation of periodate that mimics dye-sensitization of TiO₂: Simultaneous decolorization of dyes and production of oxidizing radicals. *Applied Catalysis B: Environmental*, 203, pp. 475–484.

Zangeneh, H., Zinatizadeh, A.A.L., Habibi, M., Akia, M. and Hasnain Isa, M., 2015. Photocatalytic oxidation of organic dyes and pollutants in wastewater using different modified titanium dioxides: A comparative review. *Journal of Industrial and Engineering Chemistry*, 26, pp. 1–36.

Zeng, M.X., Li, Y.J., Ma, M.Y., Chen, W. and Li, L.Y., 2013. Photocatalytic activity and kinetics for acid yellow degradation over surface composites of TiO₂-coated activated carbon under different photocatalytic conditions. *Transactions of Nonferrous Metals Society of China (English Edition)*, 23(4), pp. 1019–1027.

APPENDICES

APPENDIX A: EDX Analysis

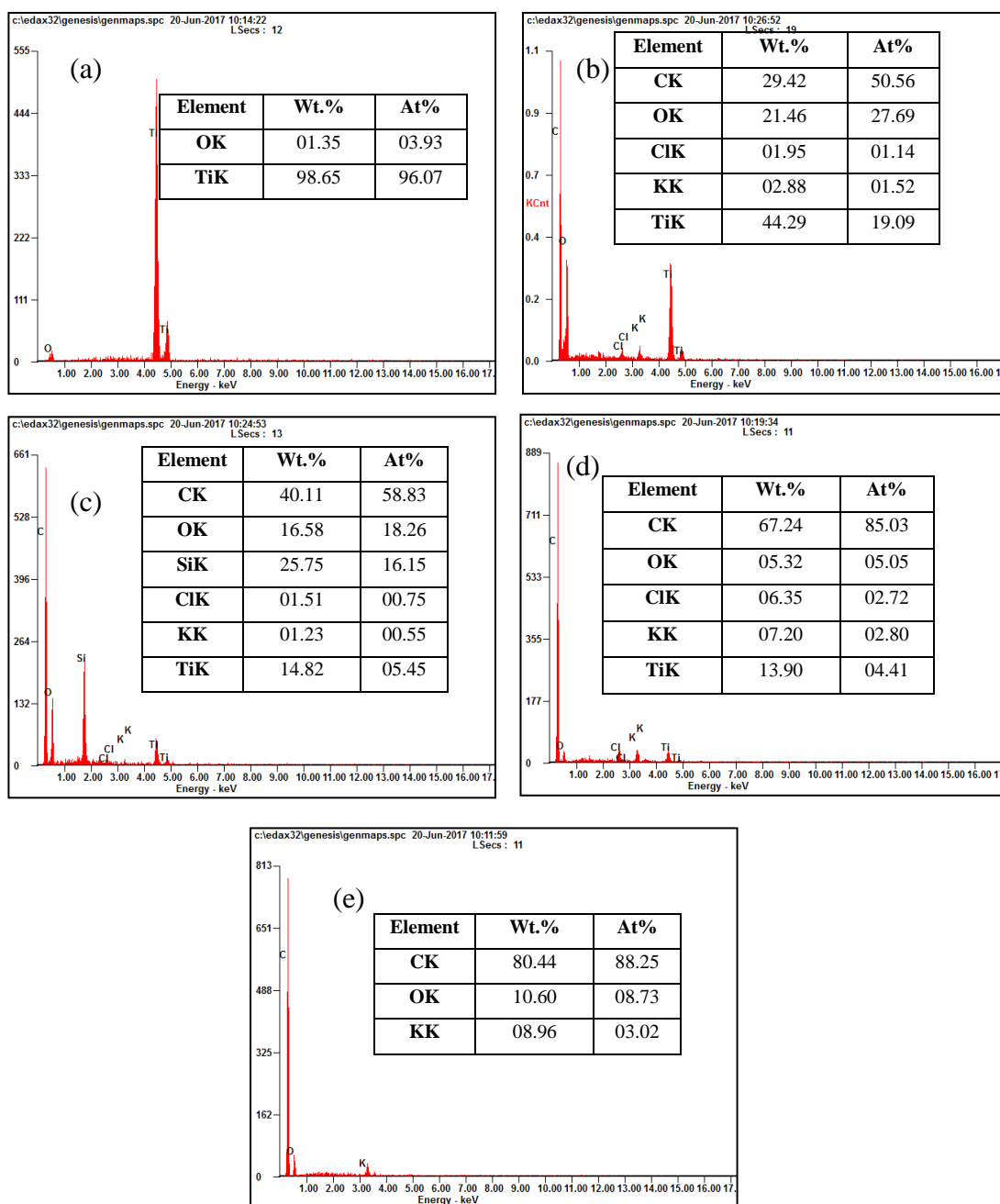


Figure A.1: EDX Analysis of (a) Pure TiO_2 , AC/ TiO_2 at Weight Ratio (b) 1:3, (c) 1:1, (d) 3:1 and (e) Pure AC

APPENDIX B: Preparation of Various Concentrations of Organic Dyes

To find out the concentration of organic dye that was required for experiment from a stock solution, dilution process was necessary. By knowing the concentration of stock solution, desired concentration and volume of organic dye, the volume from stock solution that was required can be computed by using:

$$C_1V_1=C_2V_2$$

where

C_1 = Stock solution's concentration, g/L

V_1 = Stock solution's volume, L

C_2 = Diluted solution's final concentration, g/L

V_2 = Diluted solution's final volume, L

After the value of V_1 was computed, V_1 of stock solution was pipetted and then it was diluted by adding distilled water until the volume reach V_2 value.

To prepare a stock solution of 99 % Malachite Green with the concentration of 500 mg/L in 0.5 L, the mass of Malachite Green required was calculated as shown below:

$$\begin{aligned} \text{Mass of Malachite Green} &= \frac{1}{0.99} \times 500 \frac{\text{mg}}{\text{L}} \times 0.5 \text{ L} \\ &= 2525 \text{ mg} \\ &= 2.525 \text{ g} \end{aligned}$$

Therefore, 2.525 g of Malachite Green was dissolved in 0.5 L distilled water to obtain the stock solution with concentration of 500 mg/L in 0.5 L.

The volume of 99 % Malachite Green stock solution of 500 mg/L required to prepare different concentration of organic dyes in 100 mL solution is shown in Table B.1. The volume of 99 % Malachite Green stock solution of concentration 500 mg/L required to prepare 100 mL of diluted Malachite Green solution with concentration of 10 mg/L was calculated using the following equation.

$$\left(500 \frac{\text{mg}}{\text{L}}\right) (V_1) = \left(10 \frac{\text{mg}}{\text{L}}\right) (100 \text{ mL})$$

$$V_1 = 2 \text{ mL}$$

Hence, 2 mL of Malachite Green stock solution was pipetted and then diluted by adding distilled water until the volume reached 100 mL.

Table B.1: Volume of 99 % Malachite Green Stock Solution of 500 mg/L Required to Prepare Different Concentration of Organic Dyes in 100 mL Solution

Concentration of Malachite Green (mg/L)	Volume of 99 % Malachite Green Stock Solution of 500 mg/L Required (mL)
10	2
20	4
30	6
40	8
50	10

APPENDIX C: Calibration Curve of Malachite Green

The calibration curve of Malachite Green is shown in Figure C.1.

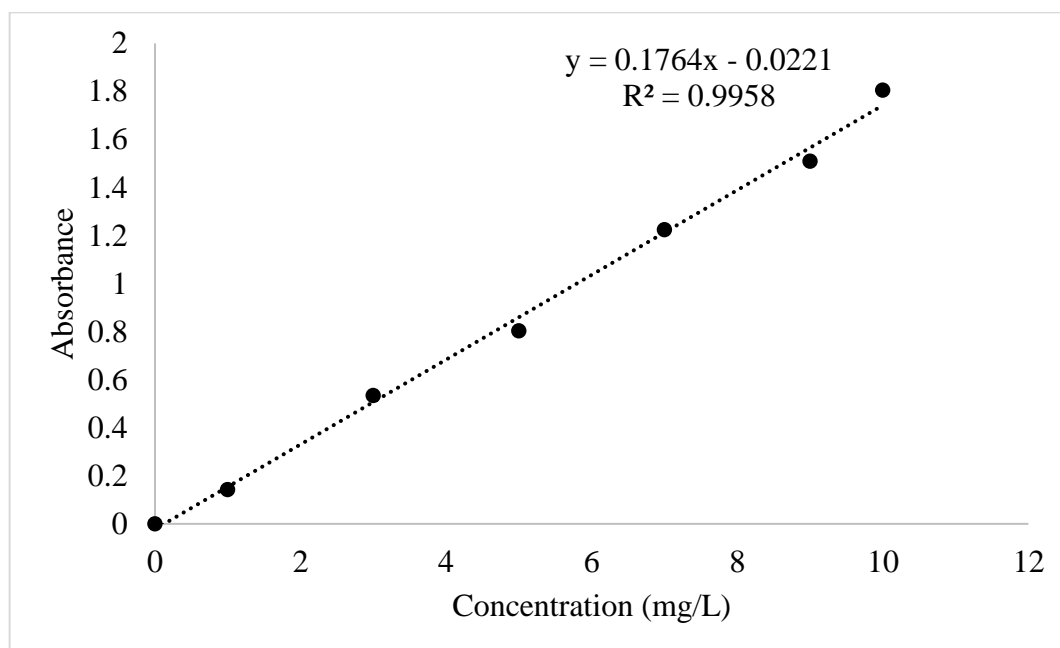


Figure C.1: Calibration Curve of Malachite Green

APPENDIX D: Calculation of Average Crystallite Sizes

The average crystallite sizes of materials can be calculated from XRD spectra by applying the Scherrer equation (Singh, et al., 2016).

$$D = \frac{K\lambda}{\beta \cos\theta}$$

where

K = Scherrer constant, 0.9

D = average crystalline size,

λ = X-ray wavelength, 0.154 nm

β = the peak width of half maximum, °

θ = Bragg diffraction angle, °

Peak data for Pure AC:

$$\beta = 0.1008^\circ = 0.001759 \text{ rad}$$

$$\theta = 21.4336^\circ$$

Crystalline size of Pure AC was calculated as shown below:

$$\begin{aligned} D &= \frac{K\lambda}{\beta \cos\theta} \\ &= \frac{0.9 \times 0.154 \text{ nm}}{0.001759 \text{ rad} \times \cos\left(\frac{21.4336^\circ}{2}\right)} \\ &= 80.18 \text{ nm} \end{aligned}$$

APPENDIX E: Reaction Kinetics Plot

The kinetics of photocatalytic degradation of Malachite Green can be described as:

Zero-order:

$$C_t = C_0 - k_0 t$$

Second-order:

$$\frac{1}{C_t} = \frac{1}{C_0} + k_2 t$$

where

C_0 = initial dye concentration, $\frac{\text{mg}}{\text{L}}$

C_t = dye concentration at time t , $\frac{\text{mg}}{\text{L}}$

k_0 = apparent pseudo zero-order rate constant, $\frac{\text{mg}}{\text{L}\cdot\text{min}}$

k_2 = apparent pseudo second-order rate constant, $\frac{\text{L}}{\text{mg}\cdot\text{min}}$

A plot of $C_0 - C_t$ against t is shown in Figure E.1 and a plot of $1/C_t - 1/C_0$ against t is shown in Figure E.2.

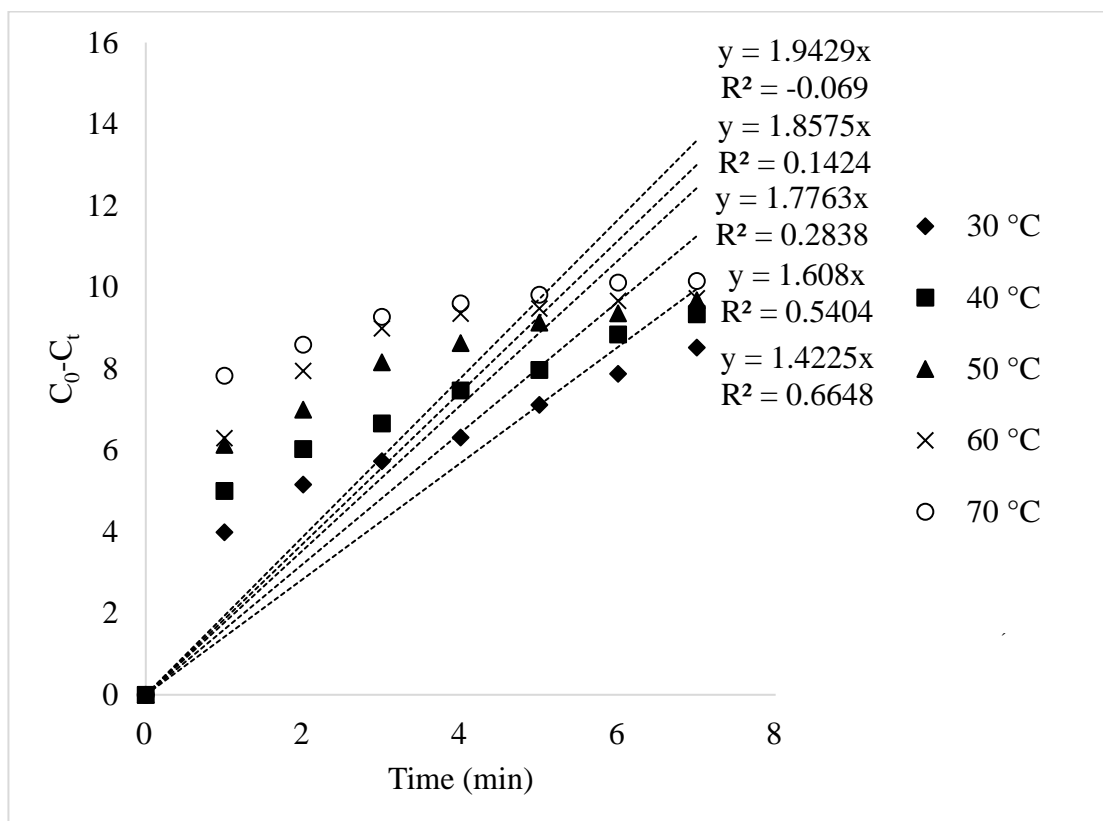


Figure E.1: Pseudo Zero-Order Reaction Kinetics Plot for Photocatalytic Degradation of Malachite Green

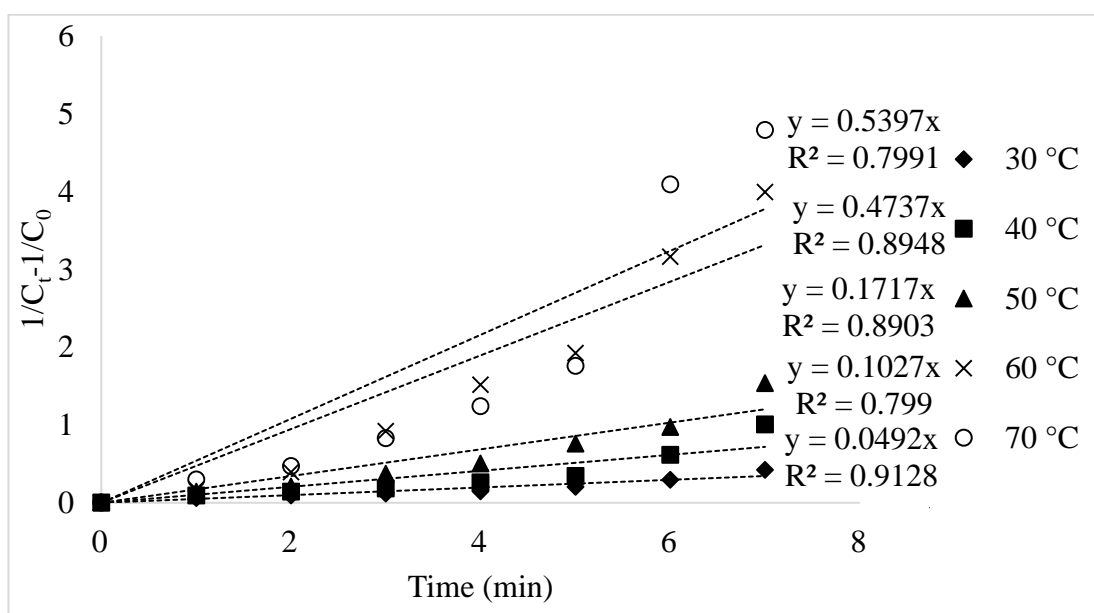


Figure E.2: Pseudo Second-Order Reaction Kinetics Plot for Photocatalytic Degradation of Malachite Green

APPENDIX F: Material Safety Data Sheet (MSDS)